Chapter 4 FTIR-ATR Diffusion Study

4.1 Introduction

Infrared spectroscopy is a widely used technique that for many years has been an important tool for investigating chemical processes and structure. The combination of infrared spectroscopy with the theories of reflection has made advances in surface analysis possible. Specific IR reflectance techniques may be divided into the areas of specular reflectance, diffuse reflectance, and internal reflectance. The latter is often termed as attenuated total reflectance and will be the focus of this work.

In this chapter, the principles behind *Fourier Transform Infrared – Attenuated Total Reflectance (ATR) Spectroscopy* are discussed. An innovative technique for monitoring the transport process of low molecular weight species was established based upon these concepts. This enabled the monitoring of individual species *in-situ*, while providing additional chemical information on any changes that may be occurring during the transport process.

An ATR-diffusion model based upon Fick's second law was developed and is described in detail in the next section. A physical apparatus was designed and built for the appropriate boundary conditions. Bulk diffusion coefficients are evaluated from the ATR data and additional insight into the chemical nature of the transport process was gained. A brief review of the current literature pertinent to the type of analysis described is given.

4.2 Theory

The fundamentals of attenuated total reflection (ATR) spectroscopy date back to the initial work of Jacques Fahrenfort and N.J. Harrick, both of whom independently devised the theories of ATR spectroscopy and suggested a wide range of applications. Therefore, it is necessary to begin our description with an evanescent wave and how it is related to the concept of internal reflection.

The concept of internal reflection spectroscopy originates from the fact that radiation propagating in an optically dense medium of refractive index n_1 undergoes total internal reflection at an interface of an adjacent medium of lower optical density (refractive index $n_2 < n_1$). This wave is termed *evanescent* and is derived from the Latin root *evanescere*, meaning "to tend to vanish or pass away like a vapor"[1]. The above phenomenon occurs only when the angle of incidence exceeds a critical angle θ_c determined by:

(1) $$\sin\theta_c = \frac{n_2}{n_1}$$

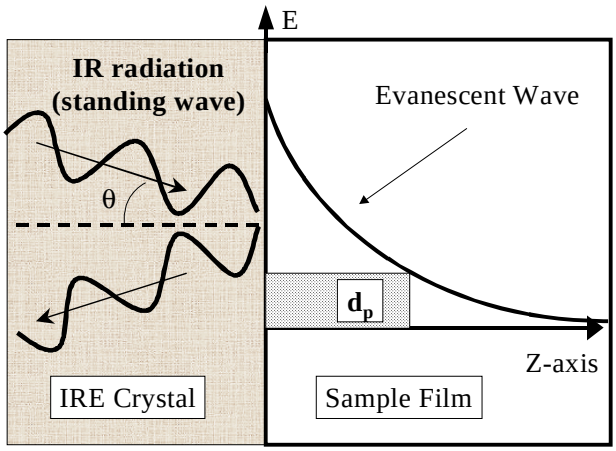

Figure 4-1. Schematic of the evanescent wave formed at the internal reflection element-sample surface. d_p is defined as the penetration depth.

The simple treatment of Figure 4-1 shows a transverse standing wave totally reflected at the interface. This wave is best described as the interference wave of the incident and reflected waves.[2] A few characteristic properties of the evanescent field are:

1) The field intensity in the medium of lower refractive index is nonzero, and there is an instantaneous normal component of energy flow into this medium whose time average is zero. Thus, there is no energy loss and the propagating radiation in the denser material is totally internally reflected.

2) The evanescent field is a nontransverse wave that has vector components in all spatial directions. This is a very unique feature and has many implications.

3) Intensity of the field decreases with increasing distance into the medium, normal to its surface. Therefore, the field exists only near the vicinity of the surface.

4) A nonzero energy flow parallel to the interface results in a displacement of the incident and reflected waves. This is known as the Goos-Hanchen shift.[1,3,4]. Many efforts have been made[4,5] to investigate the correlations between this shift and the depth of penetration or effective thickness, but nothing conclusive has resulted.

The exponential decay of the electric field amplitude (E) within the rarer medium can be described as:

(2) $$E = E_o \exp\frac{-2\pi}{\lambda_1}\left(\sin^2\theta - n_{21}^2\right)^{1/2} z$$

where E_o = initial electric field amplitude

λ_1= wavelength of radiation in denser medium = λ/n_1

λ = wavelength in free space

θ = incident angle, $n_{21}=n_2/n_1$, and

z = distance from the surface.

As mentioned earlier, the evanescent wave is nontransverse, and, therefore, has components in all spatial directions. This allows its vector components to interact with the dipoles in all orientations, causing it to be a more informative probe of the material.

So far the idea of internal reflection has been described in terms of a non-absorbing rarer medium. However, this is an ideal case since an absorption of energy, particularly in the IR spectrum, is expected in most materials. A further complication that will be discussed later is the potential of the refractive index of the rarer medium to undergo dispersion across an absorption band.

Harrick and du Pre[6] proposed a description of the distance through which the evanescent wave travels. A parameter known as the penetration depth, d_p, was defined as the depth at which the field strength, E, decays to a value of $E_o\exp(-1)$. In other words, it is the depth into the rarer medium, where the amplitude of the evanescent wave is only 37% of its original value. The actual thickness of the material sampled is, however, greater than the arbitrary d_p defined by Harrick and duPre.

Penetration depth was illustrated by Mirabella[7] using polypropylene and polystyrene (Figure 4-2 and 4-3). For both polymers on a KRS-5 (a eutectic mixture of thallium and bromide iodides) internal reflection element, the actual sampling depth was found to be approximately three times d_p. However, only 5% of the initial value of E_o or 0.25% of the original intensity remains at three times d_p. This study utilizes a very accurate measure of sampling depth, and validates the expression for electric field amplitude described above, implying that the majority of information is obtained from the lesser depths into the sample. Furthermore, the equation for the electric field is derived upon the assumption of zero absorbance, which is supported by the excellent agreement between the predicted and experimental data. Thus, it can be seen that the effect of absorption is small for most organic compounds, especially for polymers.

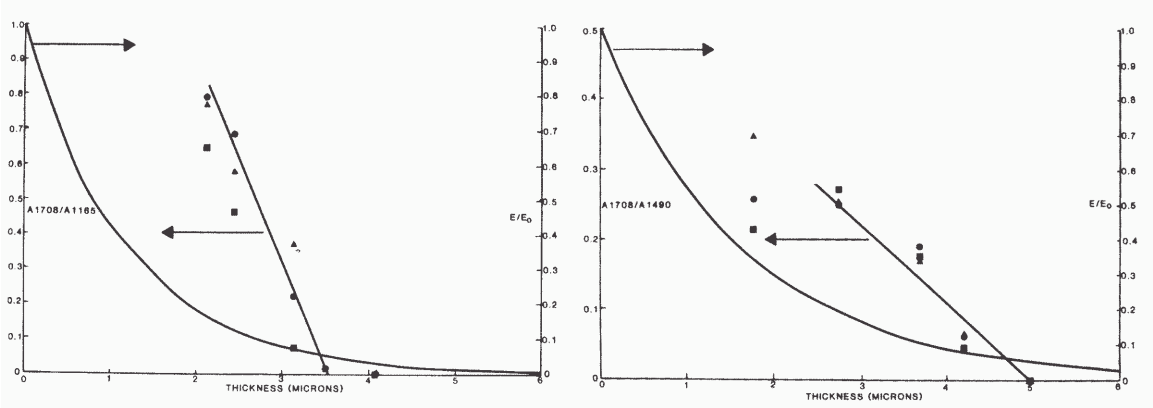

Figure 4-2 & 4-3. Absorbance ratio A_{1708}/A_{1165} (Mylar backing/PP) and A_{1708}/A_{1490} (Mylar/PS) and electric field amplitude decay at 1708cm^{-1} as a function of thickness of polypropylene layer measured via KRS-5 at 45° (ref 7).

This assumption of low absorptivity can be further treated in terms of the intensity loss per reflection. The reflectivity, R, of a non-absorbing material is given by:

(3) $$R = \frac{I}{I_o} = 1$$

where I = reflected intensity, and

I_o = incident intensity.

From transmission IR, the amount of energy transmitted, T, is defined as:

(4) $$T = e^{(-\alpha d)}$$

where α is the absorption coefficient (cm^{-1}) and d is the sample thickness. The analogous expression for reflection of a weakly absorbing species is:

(5) $$R = e^{(-\alpha d_e)} \approx (1 - A)$$

where d_e is defined as an effective thickness that yields the same absorbance levels from transmission, as are obtained from internal reflection spectroscopy. In contrast, for a strongly absorbing species with a complex refractive index, $n'=n(1+ik)$,

(6) $$\alpha = 4\pi nk / \lambda$$

where k is the attenuation index. The absorption coefficients were calculated for polypropylene[7] (n=1.5) on a KRS-5 IRE with an incident angle of 45°. An effective

thickness per reflection = 4.05μm, and an absorbance per reflection of the 1165cm^{-1} band = 0.05, were inserted into equations (5) and (6) to yield α=288 cm^{-1} and k=0.013. These numbers are far below the maximum values, over which the zero absorption approximation is invalid ($\alpha \leq 10^4$; $k \leq 0.1$). Therefore, the assumption of a weakly absorbing species is valid for most organics, including polymers.

4.3 Experimental Considerations

All of the internal reflection theories are based on energy transfer between media of lower and higher refractive indices. Therefore, it is crucial that contact between the two media be as intimate as possible, which gives rise to a new technical complication not experienced in normal transmission spectroscopy. Typical methods for insuring such a contact are (a) casting of films upon the IRE crystal and (b) a physical clamping device. The latter involves a *clamping pressure* that is an experimental parameter whose control is of immense significance to the results obtained. Figure 4-4 illustrates the influence of this parameter on the peak intensities of the IR spectrum of polypropylene[8].

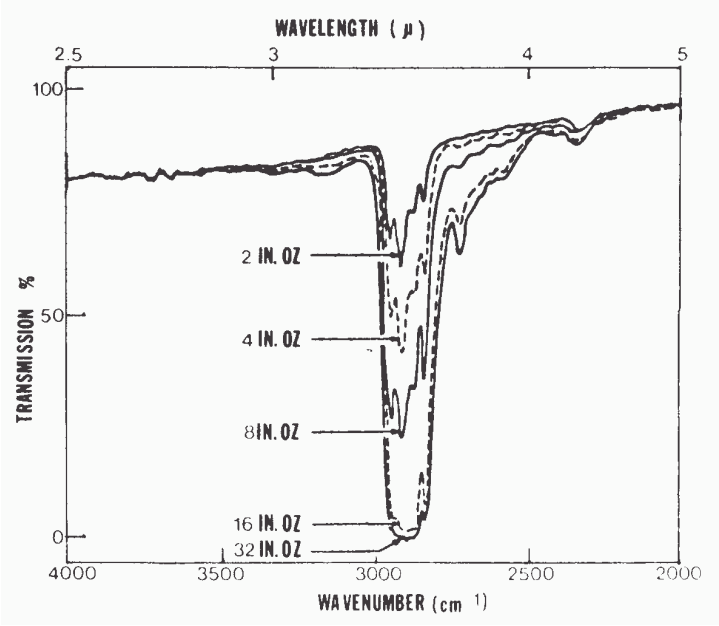

Figure 4-4. Effect of contact pressure on polypropylene spectra on KRS-5 at 45°. Values refer to torque wrench settings. (ref.8)

Other experimental factors include crystal type and angle of incidence. Crystal types vary greatly, and characteristic features of a few are given below:

Table 4-1. IRE Materials Used in ATR Applications

Material	Refractive Index ($1000cm^{-1}$)	Spectral Range (cm^{-1})
Zinc selenide	2.4	20,000-650
AMTIR (As/Ge/Se glass)	2.5	11,000-750
Germanium	4.0	5,500-870
KRS-5 ($TlI_2/TlBr_2$)	2.37	20,000-350
Zinc sulfide (ZnS)	2.2	17,000-950
Cadmium telluride (CdTe)	2.65	10,000-450
Sapphire (Al2O3)	1.74	25,000-1800
Cubic Zirconia (ZrO2)	2.15	25,000-1800
Diamond	2.4	45,000-2500; 1650-<200

The last variable, *angle of incidence*, (θ) is governed by the obvious requirement that it be at least as great as the critical angle, θ_c. It is largely determined by the material properties of the polymer and the crystal. Previous studies[9] have shown a strong influence of θ on the effective penetration depth (d_p) that is much stronger in the vicinity of θ_c. The importance of being consistent with regard to the angle of incidence, especially near the critical angle during the experiment, has also been emphasized.

From the above discussion, it is clear that careful consideration of *all* the parameters that may affect the quantitative analysis of FTIR-ATR spectroscopy is essential for good results. In the current research, all of the above factors were meticulously accounted for, in order to accurately evaluate the diffusion properties of the polymer studied. The adhesive films were cured directly onto the IRE with a constant pressure of about 10 psi, ensuring excellent contact between the two materials. Also, a clamping mechanism with a constant clamping pressure was used for all experiments. An IRE crystal of ZnSe was selected due to its ease of availability and its ability to survive the curing and cleaning processes. A constant angle of incidence of 45° was utilized. As will be discussed later, this is relatively close to the critical angle of the adhesive, thereby maximizing the penetration depth of the analysis.

4.4 Quantitative Considerations

The *in-situ* evaluation of diffusivity is dependent upon the ability to quantify the FTIR-ATR spectra obtained. The IR absorbance values of a sample are related to its concentration, analogous to the way concentration is related to absorbance in transmission spectroscopy through the Beer-Lambert law. However, the inherent features of internal reflection spectroscopy, some of which will be addressed below, render such a quantitative analysis very complicated.

4.4.1 Wavelength Dependence

From the expression for penetration depth, it can be seen that d_p is related to the wavelength of radiation (λ). This in turn results in a proportionality between λ and effective depth. Thus, in the internal reflection spectra of bulk materials, the absorption bands at longer wavelengths are relatively more intense than those at shorter wavelengths. This results in greater absorption on the longer wavelength side of an absorption band, contributing to band distortion. For broad bands, this broadening effect is accentuated and may result in a peak shift to longer wavelengths.

4.4.2 Dispersion Effects

Dispersion is a term used to describe the change in refractive index (*n)* of a material with wavelength (λ). Normal dispersion phenomena can be described as a continuous decrease in *n* with increasing λ[10] and is typical of optically transparent (non-absorbing) materials. For a material that can absorb energy, the refractive index undergoes what is known as an anomalous dispersion as illustrated in Figure 4-5. The anomaly is the fact that *n* is higher at longer wavelengths in a region of absorption, contrary to what is expected.

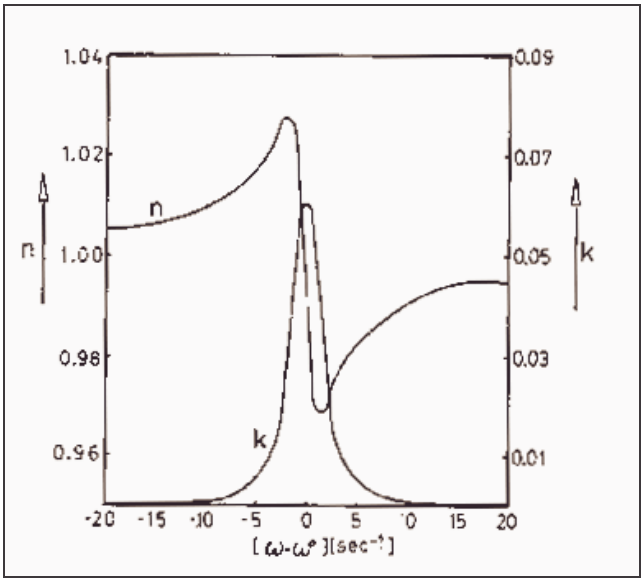

Figure 4-5. Plot of *n* and *k* spectra during an absorption band at frequency ω_o.

The dispersion in the vicinity of the absorption bands is a well-known phenomenon in transmission and external reflection spectroscopy. It also plays an important role in the nature of internal reflection spectroscopy. The effect of dispersion on the resulting ATR spectrum has been demonstrated by Mirabella[11] with measurements on polypropylene near the critical angle (Figure 4-6). In an attenuated total reflection experiment, the resulting absorption spectrum is not a true measure of either the

absorption index (k) or the refractive index (*n*). Instead, it is a complex function of both, as was described in equation (6). According to the dispersion shown in Figure 4-6, this spectrum shows the combined effects of the *n*-spectrum and the *k-spectrum*, in the form of band asymmetry. An added complication arises from the fact that the anomalous change in refractive index also changes the critical angle and penetration depth throughout an absorption band, which can enhance the optical effects.

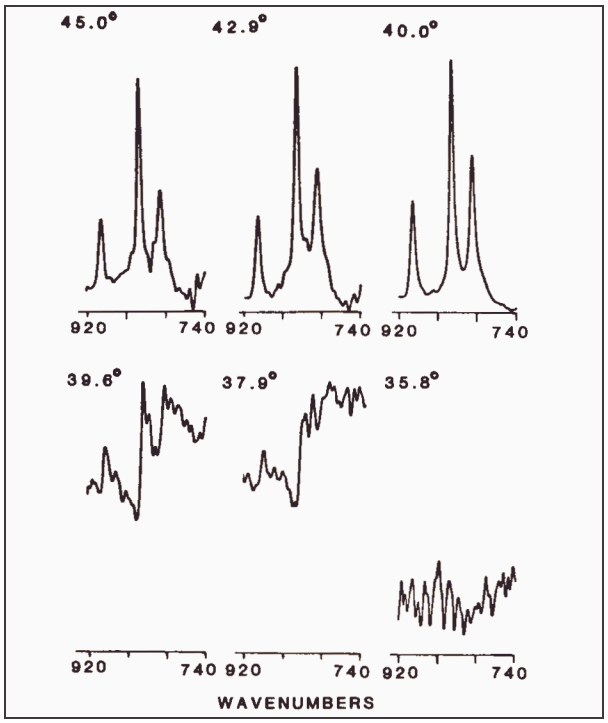

Figure 4-6. ATR-IR Absorption Near Critical Angle of Polypropylene on KRS-5 IRE. (ref.11)

Since the influence of optical dispersion on transmission spectroscopy (TS) is typically small, it is often ignored. However, Graf, Koenig, and Ishida[12] have shown (by means of a Kramers-Kronig analysis) that the intensity and the extent of interference fringes in a transmission spectrum of thin polymer films are greatly affected by optical dispersion. Similar results have also been obtained by Greenler[13] and Francis and Ellison[14].

Nishikida and Hannah[15] have confirmed the fact that the optical effects in reflection spectroscopy (RS) are much greater than those on TS. The 960 cm^{-1} peak for γ-Al_2O_3 acquired through grazing angle reflection corresponded to an absorption band at 738 cm^{-1} from TS. In addition, a weak band around 700 cm^{-1} was also attributed to a 590 cm^{-1} transmission peak. The refractive index (*n)* was calculated using the Kramers-Kronig relationship assuming *k* is equivalent to the experimental absorption spectrum. Theoretical predictions by Allara *et al.*[16] of a shift in the C=O stretch of poly(methyl

methacrylate) due to optical dispersion effects was substantiated by the 10 cm^{-1} shift in the carbonyl stretch of PMMA on a gold substrate. Ishida *et al.*[12,17] demonstrated that accurate values for the optical constants of poly(styrene), poly(methyl methacrylate) and poly(vinyl chloride) could be obtained by accounting for optical dispersion.

Optical effects have also been shown to yield peak splitting, as in the case of Mylar on silicon substrate.[18] A band at 1740 cm^{-1} split into two (1786 cm^{-1} and 1515 cm^{-1}) absorption bands. Methods such as asymmetric curve fitting[19] have been incorporated to resolve the spectral distortions. However, it is essential to mention that these are simply mathematical manipulations with no theoretical basis. For an in-depth review on optical dispersion effects, the reader is referred to the work of Harrick.[17]

Urban and Huang[20] have investigated the effects of overlapping bands on the observed intensities from FTIR-ATR. Although band ratioing techniques are commonly used in transmission IR to establish relative concentrations in mixtures,[21,22] the situation changes drastically when looking at films using internal RS. Simulated results showed how overlapping bands in TS could be resolved easily and accurately for band separation gaps of at least 4 cm^{-1}, while the ability to resolve the ATR spectra is greatly influenced by the band separation gap. A comparison of the two spectra is given in Figure 4-7 and Figure 4-8, wherein, both peaks *a* and *b* should be of equal intensity. The ability to resolve the individual peaks improved with increasing band separation. In the ATR spectra, when the band separation exceeded 30 cm^{-1} (or twenty times the half-width at half-maximum (HWHM)), the intensity changes leveled off. For larger separations, the effect of wavelength on penetration depth may become more dominant. Hence, there are two opposing factors that must be considered. A band separation of approximately 20 times HWHM was estimated to be sufficient in order to neglect overlap effects.

All of the above considerations are important and must be included in the current study, wherein the change in absorbance with time will be monitored in order to determine diffusion coefficients. To aid in the evaluation of this relative change, a ratioing technique[23] will be utilized. The caveats described earlier for overlapping bands are not applicable since the band separation is greater than 110 cm^{-1}. According to Urban[20], this separation is sufficient to minimize both the peak dispersion and intensity ratio errors, and the penetration depth dependence. These factors will be accounted for in the actual analysis of the experimental data.

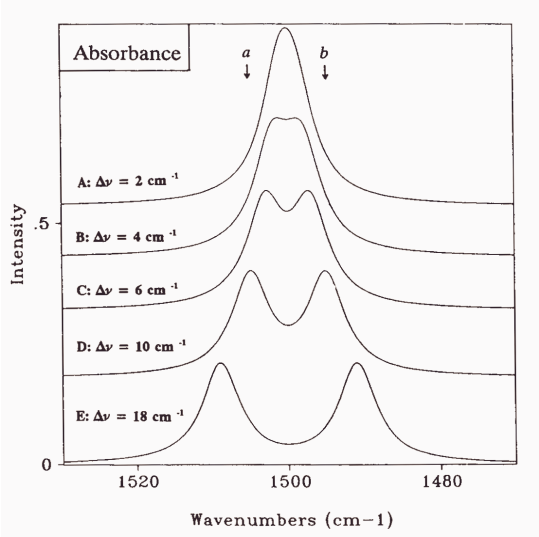

Figure 4-7. Simulated absorbance spectra *k*max=0.25 intensity. Band separation distance is designated as Δν. (ref.20)

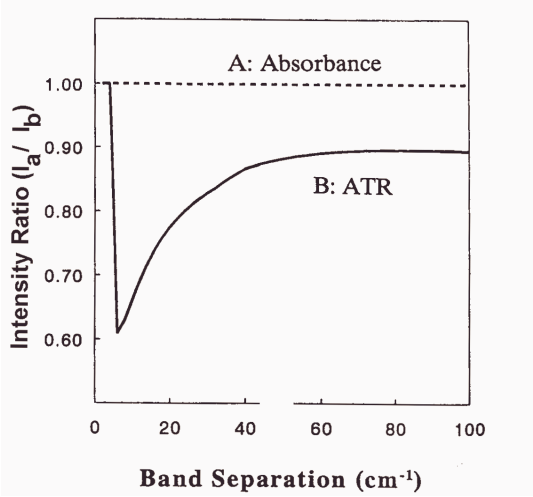

Figure 4-8. A Plot of Intensity Ratio as Function of Band Separation, Δν. (ref.20)

4.5.0 Literature Survey

In the study of polymers, most applications for Fourier transform infrared-attenuated total reflectance (FTIR-ATR) spectroscopy involve the characterization of a polymer surface or a liquid solution[11,18,24,25]. The development of ATR spectroscopy as a powerful technique for monitoring diffusion behavior within polymers is relatively new. Conventional methods involve periodic sampling and subsequent analysis by either weighing, spectroscopic, chromatographic, or even radiometric means. In contrast, FTIR-ATR allows for the direct and unequivocal identification and quantification of the penetrant and its concentration in a polymer film, *in-situ*. This feature enables experiments to continue undisturbed, insuring the accuracy of the experiment. A degree of "*contrast*" is necessary to distinguish the permeant from the matrix and arises from the differences in the vibrational spectra of the two materials.

The original concept of ATR spectroscopy as a tool for monitoring diffusion dates back to the early adhesion studies by Vorenkamp *et al*.[26]. They observed an increase in the carbonyl stretching band of poly(methyl methacrylate) as it diffused into a layer of poly(vinyl chloride) using this technique. However, they did not quantify this observation nor calculate a diffusion coefficient.

Quantification of the transport process was attempted by Remizov *et al*.[27] on small molecule diffusion into polyethlyene, and by Kausch and Jud[28] on polymer interdiffusion of polystyrene and polyacrylonitrile. Neither of these studies was successful since the exponentially decaying nature of the evanescent field was not accounted for. Also, the experiments were not carried out *in-situ*, thereby allowing extensive experimental error.

Many different relationships to evaluate diffusion coefficients have been developed for FTIR-ATR spectroscopy. All of them involve the basic methodology of solving a set of boundary conditions for the diffusion equation in order to yield an expression describing the temporal dependence of the concentration profile (e.g. Crank[29]). For case I or Fickian diffusion, this profile C(z,t) is solved assuming that mass flux is proportional to the penetrant concentration gradient. For a case II diffusion such as that seen in a glassy polymer, the gradient between the two phases is very sharp and typically advances with a constant velocity. The model that best describes the system should be used, in conjunction with the appropriate quantitative expressions for ATR spectroscopy. The most common application of this technique has been the study of the diffusion behavior of low molecular weight species. Their diffusion coefficients are evaluated by analyzing the absorbance spectra obtained based on a suitable model.

Schottler and Furlan[30] originally proposed a less direct means of calculating the diffusion coefficient (D) of n-decyl alcohol in hydrogenated polybutadienes. Mass uptake profiles were calculated using predicted diffusion coefficients and a Fickian model. Absorption intensities of the alcohol were experimentally collected and the contribution of the alcohol was deconvoluted from that of the evanescent field. Correction for the electric field effect yielded an intensity that could be directly compared

to the mass uptake profile. An adjustable time constant defined as $(d_s)^2/D$, where d_s is the sampling depth, was used to obtain the best fit of the two curves. This analysis demonstrated the effect of the branch content of polybutadiene on its crystallinity and diffusion coefficient due to the changes in "tortuosity."

A subsequent study[31] was carried out to test the applicability of the "tortuosity" concept and the use of a two-phase model to describe crystallinity and its effects on diffusivity. Gross deviations from this model were observed and attributed to the existence of partially ordered regions that behaved in a manner intermediate to that of purely crystalline and purely amorphous phases. Although the methodology utilized is technically sound, it suffers from the disadvantages of being indirect and cumbersome to use.

A simpler means of evaluating diffusivity (D) of low molecular weight species in glassy polymers has been developed by Fieldson and Barbari[32]. Liquid water was allowed to diffuse into polyacrylonitrile (PAN) at room temperature on a silicone IRE. As the temperature of treatment increased, the amount of water sorbed as well as the equilibrium IR absorbance decreased. However, this was accompanied by an increase in diffusivity. This behavior was due to the presence of residual DMF solvent within the PAN further emphasizing the importance of polymer processing. The model derived in this study utilized a 1-dimensional "thin-film" solution, which converged to a simple mathematical form. A detailed *error analysis* was included to demonstrate the validity and reproducibility of the technique. Furthermore, deconvoluting the water spectra into its monomeric and clustered forms was suggested.

Since polyimides are well known for the ease with which they permit transport of water, most of the diffusion studies on this material are concerned with the influence of the polymer structure on water transport[33,34,35,36,37,38,39,40]. For example, changes in morphology and density of a semicrystalline polyimide were induced by means of different thermal curing cycles. Diffusion coefficients were found to be strongly dependent upon chain stiffness, level of crystallinity and density of the amorphous phase. The activation energies of diffusion could not be easily correlated to any degree of chain stiffness or orientation- a complex combination of the two parameters was suggested. The *in-situ* ATR spectra also quantified the increased hydrogen bonding within the system. It also denoted a bimodal distribution of water sites of presumably single and clustered water molecules, thus proving to be a very sensitive probe to any specific interactions within the material.

FTIR-ATR has also become a valuable tool in the medical field for quantifying drug adsorption and controlled-release delivery systems of therapeutic agents. Farinas *et al.*[41] applied a simple ATR diffusion model analogous to the "long-time" approximation utilized in mass uptake procedures, to the study of diffusion of urea into a silicone pressure-sensitive adhesive. A band ratioing technique[1,18,42] with an internal standard was used for the compensation of changes in polymer/optical contact during the experiment. Furthermore, complimentary radioisotope measurements of diffusion were

performed with ^{14}C labeled urea, providing a direct comparison of the ATR technique to an independent method.

A major area of interest for diffusion-based ATR models is the effect of water on adhesion. This is due to the fact that water is the main cause of corrosion, blistering and debonding of organic coating/substrate systems. T. Nguyen *et al.*[43,44,45] have extensively analyzed the problem of water diffusing to a polymer/substrate interface using the high-energy surface of an IRE element as the substrate (Ge, KRS-5, and silicone). They developed a method based upon a two-layered system that was derived rigorously from internal reflection theory taking into account:

(1) water at the coating/substrate interface,
(2) water taken up by the coating within the probing depth of the evanescent wave, and
(3) change in penetration depth as water displaces the coating from the substrate.

Gravimetric means were utilized to construct absorbance vs. time relationships for both an epoxy and alkyd resin. The experimental spectra were assumed to be due to the combined absorbances of water in the film and at the interface. Any additional contributions to the spectra were categorized as arising from interfacial water. The model also considered the polymer film moving away from the penetration depth, d_p, of the infrared radiation, due to the formation of a water-polymer layer at the boundary. This depth was corrected for the strong absorbance of water using an expression from Muller *et al.*[46] and the diffusion coefficients were evaluated using a time-lag model for ATR spectroscopy. The extent of adhesion between the polymer and substrate was qualified in terms of the thickness of the water layer formed.

Skourlis and McCullough[47] have investigated the diffusion of a liquid diamine curing agent (*bis*(p-amino cyclohexyl) methane) into an epoxy prepolymer, on a cylindrical Ge crystal whose geometry was approximated with Cartesian coordinates. Diffusivity was obtained as a function of temperature using a one-parameter Fickian model. The Arrhenius equation was used to describe the prediction of stoichiometric gradients during the curing reaction. This work also illustrated that minor errors in the calculation of the refractive index of a material result in only minor changes in the penetration depth (d_p) without affecting the diffusivities significantly.

Several investigations take advantage of the unique capability of ATR spectroscopy to unequivocally identify individual species. A good example is the study on the multi-component diffusion of methyl ethyl ketone (MEK) and toluene mixtures into polyisobutylene[48]. Vapor sorption of the components of the mixture were monitored via the carbonyl band (1723 cm^{-1}) of MEK and the aromatic absorption (1605 cm^{-1}) for toluene. A detailed and rigorous derivation for the ternary process, involving an additional term in the diffusion continuity equation for the second penetrant, was given. It yielded four different diffusion coefficients, two of which are “cross-terms” that are assumed to be negligible compared to the “main” coefficients. Thus, the model could be reduced to two independent binary diffusion coefficients. It was demonstrated that the

transport of the faster component (MEK) was affected to a very small extent by the existence of the third phase. However, the slower component (toluene) was influenced greatly by the concentration gradients of both the penetrants as well as by the additional free volume introduced by the faster penetrant.

ATR-diffusion analysis is also applied in the area of polymer-polymer interdiffusion. McKnight and Gillespie[49] have studied the diffusion of water into a polypropylene-silane interphase. A double layer consisting of a 0.5 μm thick silane primer and a 100 μm thick PP was cast onto an IRE. A Laplace transform was performed on the governing differential equations and boundary conditions for this geometry followed by an inverse transform to obtain the solutions in real space. Concentration profiles for each layer were solved using the diffusion coefficients (D) of water in the pure films. It was possible to approximate D for the bilayer using a single-film model. This was possible since the rate-determining step was the diffusion through the PP or thicker layer. Simulated absorbance curves were created using the concentration profiles derived and compared successfully to the actual data and single-film model to check the validity of this approximation. Examination of the spectra revealed that the silane layer had formed a siloxane network, and that extensive hydrolysis had occurred at its interphase. This study highlights the depth of information that can be obtained from an *in-situ* experiment of this type.

Most diffusion-ATR models assume the boundary condition that the surface concentration is a constant throughout the experiment. This assumption is valid only when the penetrant originates from an "infinite reservoir." However, in the case of a polymer absorbing a single penetrant from a liquid mixture, the concentration of that penetrant in the liquid at the polymer-liquid surface may not be the same as its concentration in the bulk liquid. An analytical solution to this "mass transfer boundary layer in adjacent phase" problem was provided by Fieldson and Barbari[50]. They developed a model that was strongly dependent upon the equilibrium partition coefficient and a parameter known as the *boundary layer resistance*, α. As α approached infinity, the solution converged to that of a constant surface concentration.

The study of case II diffusion based on the mathematics of evanescent field spectroscopy is a very complex process. Fieldson and Barbari[50] have applied the simplest case of a constant surface concentration and a constant velocity front to reveal the main features of the absorbance curves and to compare them to those of a Fickian case. The concentration profile was defined using a Heaviside function and integrated into the absorbance equation for FTIR-ATR spectroscopy, resulting in an exponential dependence of absorbance with time. The model was tested using a system of methanol and poly(methyl methacrylate). Experimental values for the velocity front corresponded exactly to those reported by Grinsted *et al.*[51] using NMR. In addition to being able to differentiate monomeric and associated methanol spectroscopically, the results definitively showed how the different modes of diffusion could be easily distinguished.

Polymer interdiffusion is governed mainly by the enthalpy of mixing, in sharp contrast to low molecular weight species diffusion, which is dominated by a large entropy

of mixing. It has been extensively studied using a variety of techniques such as NMR[52,53], radioactive tracers[54,55], secondary ion mass spectroscopy,[56] and conventional IR methods[57,58]. A polymer-polymer diffusion where the permeant is much faster than the matrix may be approximated to the transport of a low molecular weight species. An example is the diffusion of a liquid epoxy resin into polystyrene[59]. Diffusion coefficients were evaluated, and variable angle FTIR-ATR was introduced to create a concentration-depth profile of the epoxy in the PS matrix by means of an inverse Laplace transform. This resembled the true composition profile evaluated independently, with transitions occurring at the appropriate spatial locations.

Due to the sluggish nature of polymer diffusion, it is often advantageous to monitor the dissolution of a thin polymer film (the diffusing species) from the surface of an IRE into an adjoining thick polymer matrix. A common Fickian model (equation (7)), with thicknesses *a* and *b*, quantifies the *loss* of the penetrant from the ATR detection volume.

$$\frac{A_t - A_o}{A_\infty - A_o} = 1 - \frac{\frac{2}{\pi}\sum_{n=0}^{\infty}\frac{\sin(n\pi\frac{b}{a})}{n}\exp\left(-n^2\pi^2\frac{Dt}{a^2}\right)\left[\frac{1+(-1)^{n+1}\exp(\frac{-2a}{\lambda})}{1+\left(\frac{n\pi\lambda}{2a}\right)^2}\right]}{\left[1-\exp\left(\frac{-2b}{\lambda}\right)\right]-\frac{b}{a}\left[1-\exp\left(\frac{-2a}{\lambda}\right)\right]} \qquad (7)$$

FTIR-ATR is widely used in studying the interdiffusion of amorphous polymers at temperatures above the higher of the two T_g's. Alsten and Lustig[60] investigated the diffusion of *d*-PMMA into a PMMA matrix and various molecular weight *d*-polystyrenes into a higher molecular weight polystyrene matrix. Simple, Fickian-type solutions were utilized to provide information regarding temperature and molecular weight dependencies. Comparison of the results to an independent study by Whitlow and Wool[56] using secondary ion mass spectroscopy (SIMS) yielded good agreement.

More complex applications involve the non-Fickian diffusion of polystyrene into poly(vinyl methyl ether) at different temperatures[61]. The interdiffusion coefficient was intermediate to the self-diffusion coefficients, but was not dominated by one component. However, in some instances, a combination of Fickian and case II transport was observed. It was concluded that in compatible polymer pairs, upon intimate contact between the two, the faster polymer component tends to swell the slower matrix as they both diffuse across the interface.

The effects of crystallinity and morphology may also complicate the transport process. Semicrystalline materials are often used as hot-melt adhesives having semicrystalline structures that are relied on to impart desired mechanical and thermal properties. Therefore, polymer interdiffusion into a semicrystalline material plays a significant role in determining its bond performance. This proved to be the motivation

for a study[62] on the diffusion of poly(ether imide) into a semicrystalline poly(aryl ether ketone ketone) matrix. Mutual diffusion activation energy increased from 9 kcal/mole for the purely amorphous polymer to 30 kcal/mole for the highly crystalline case, indicative of reduced matrix mobility. Two distinct time scales of sorption kinetics were observed. The early transport appeared Fickian, although the amount imbibed was far below that expected in the purely amorphous polymer. The longer-time kinetics were non-Fickian and identified with a time scale over which macromolecules experience "bottlenecks" between crystalline regions. It was postulated that the two sorption time scales were a result of heterogeneous restrictions along the diffusion pathways.

A similar dual time scale process was observed by Alsten *et al.*[63] in the transport of deuterated *a*-polystyrene into *a*-polystyrene and *i*-polystyrene semicrystalline matrices. The short-time transport was influenced by molecular weight and followed the scaling laws of reptation theory. Transport in the later stages was interpreted in terms of restricted regions between crystallites. Computer simulations of polymer dynamics by Muthukumar and Baumgartner[64] support this concept.

From the above review, it is clear that FTIR-ATR is an extremely versatile and informative technique in the study of bulk transport and interfacial properties. One of its major advantages over transmission spectroscopy is the ability to deconvolute a concentration profile from experimental results. Additional information on specific interactions, chemical reactions, delamination, etc. is also available from the vibrational spectra. The wealth of information that can be obtained from a single experiment, *in-situ*, makes it an attractive tool with tremendous potential.

In the current research, an appropriate diffusion model based on a "thin-film" solution for a low molecular weight penetrant has been developed. It is discussed in detail in the following section, along with a description of the technique that has been devised in this laboratory.

4.6 Development of an FTIR-ATR Diffusion Model and Technique

Traditional methods of evaluating the rate of diffusion of low molecular weight liquids in polymers usually involve gravimetric means. Other techniques including dielectric analysis[65], pulsed-field NMR[66], photoacoustic FTIR[67] and near-infrared luminescence spectroscopy[68] have also proven to be effective probes in such studies. The kinetics of diffusion of many liquid penetrants is described by Fick's second law, and are termed one-dimensional in situations where the thickness of the matrix is much less than its width or length i.e., large surface area to thickness ratio. This neglects any diffusion that may occur through the sides. Then, the solution to Fick's second law for a concentration-independent diffusion coefficient (D) is:

$$\frac{M(t)}{M_\infty} = 1 - \frac{8}{\pi^2}\sum_{n=0}^{\infty}\frac{1}{(2n+1)^2}\exp\left[\frac{-(2n+1)^2\pi^2 Dt}{4l^2}\right] \tag{8}$$

where M(t) = the weight of the polymer at time *t*,
M_∞ = the equilibrium mass uptake, and
l = one half the thickness of the polymer film.

FTIR-ATR spectroscopy has been shown to be highly effective and sensitive in the study of transport phenomenon. Its theory has been reviewed in detail in section 4.2 of this chapter. Some of its distinct advantages include:

1) the *in-situ* nature of the measurement of concentrations with time,
2) shorter experimental times than more conventional techniques,
3) small penetration depths (~ 0.1-2 μm) that permit a more surface-sensitive analysis,
4) the ability to observe chemical effects that may be occurring during an experiment, and
5) the possibility of monitoring multiple species, simultaneously.

In order to obtain quantitative information from ATR spectroscopy, the evanescent wave field strength equation should be combined with the familiar Beer-Lambert law for transmission spectroscopy. In doing so, it is necessary to assume that only weak absorption occurs. Then,

(9) $$\frac{I}{I_o} = e - A \approx (1 - A)$$ or,

(10) $$dI = -I_o dA$$

Substitution of equation (10) into the differential form of the Beer-Lambert law and subsequent integration yields:

(11) $$A = \int_0^L \frac{\varepsilon C I}{I_o} dz$$

where ε = absorption coefficient,
I = intensity, and
C = concentration of the absorbing species.

The limits of integration, 0 to L, are reflective of the diffusion of the penetrant through the thickness of the film, from one side. Since intensity (I) = E^2, where E is the field strength of the evanescent wave, and equation (11) can be combined to yield an expression for multiple reflections, N, as:

(12) $$A = \int_0^L N\varepsilon^* C E_0^2 \exp(-2\gamma z) dz$$

where $\varepsilon^* = \varepsilon / I_o$. Equation (12) is the expression analogous to the Beer-Lambert law for ATR spectroscopy. It directly relates changes in concentration to those in the absorbance

spectrum, during the experiment. To utilize this technique for evaluating the kinetics of a diffusion process, the physics of spectroscopic theory must be incorporated with a suitable diffusion model.

Equation (13) is a solution to the set of boundary conditions for a "thin-film", and is based on Fick's second law[69].

$$\frac{C(z,t)}{C_\infty} = 1 - \frac{4}{\pi}\sum_{n=0}^{\infty}\frac{(-1)^n}{2n+1}\exp\left[\frac{-D(2n+1)^2\pi^2 t}{4L^2}\right]\cos\left[\frac{(2n+1)\pi z}{2L}\right] \tag{13}$$

where 2L = thickness of the film
C_∞ = equilibrium concentration of penetrant in the film, and
D = concentration-independent diffusivity.

This equation assumes that the initial concentration within the film, $C_{(z=2L,\ t=0)}$ = 0, and that no penetrant diffusion occurs at the boundary, z = 0. This assumption is justified by the fact that the ATR-IRE crystal surface exists at the Cartesian coordinate of x = 0.

In order to derive a single expression relating IR absorbance to diffusivity, a term K is defined as:

$$K = \frac{A_t}{A_\infty} \tag{14}$$

where A_t = absorbance at time t
A_∞ = absorbance at infinite time.

Substituting the appropriate expressions for absorbance yields:

$$K = \frac{\int_0^L N\varepsilon^* C E_o^2 \exp(-2\gamma z)dz}{\int_0^L N\varepsilon^* C_\infty E_o^2 \exp(-2\gamma z)dz} = \frac{\int_0^L C\exp(-2\gamma z)dz}{\int_0^L C_\infty \exp(-2\gamma z)dz} \tag{15}$$

This can be rewritten as:

$$K = \frac{\int_0^L C\exp(-2\gamma z)dz}{\int_0^L C_\infty \exp(-2\gamma z)dz} = \frac{\int_0^L C\exp(-2\gamma z)dz}{B} \tag{16}$$

where $B = \int_0^L C\infty \exp(-2\gamma z)dz$.

Integration of B gives,

$$B = \int_0^L C\infty \exp(-2\gamma z)dz = C_\infty \left[\frac{1}{-2\gamma}\exp(-2\gamma z)\right]_0^L = \frac{C_\infty}{-2\gamma}[\exp(-2\gamma L)-1]$$
$$= \frac{C_\infty}{+2\gamma}[1-\exp(-2\gamma L)] \quad (17)$$

On substituting equation (17) into equation (16),

$$K = \frac{\int_0^L C\exp(-2\gamma z)dz}{\frac{C\infty}{2\gamma}[1-\exp(-2\gamma L)]} \quad (18)$$

The physics of diffusion is incorporated into the derivation, by defining the concentration profile as a Fickian case, as in equation (13). Solving for C and subsequent substitution into equation (18) yields:

$$K = \frac{\int_0^L C_\infty \left[1-\frac{4}{\pi}\sum_{n=0}^{\infty}\frac{(-1)^n}{2n+1}\exp\left[\frac{-D(2n+1)^2\pi^2 t}{4L^2}\right]\cos\left[\frac{(2n+1)\pi z}{2L}\right]\exp(-2\gamma z)\right]dz}{\frac{C_\infty}{2\gamma}[1-\exp(-2\gamma L)]} \quad (19)$$

This can be further simplified to:

$$K = 1 - \frac{\int_0^L \frac{4}{\pi}\sum_{n=0}^{\infty}\frac{(-1)^n}{2n+1}\exp(g)\cos(fz)\exp(-2\gamma z)dz}{B'} \quad (20)$$

where $B' = \frac{1}{2\gamma}[1-\exp(-2\gamma L)]$,

$$g = \frac{-D(2n+1)^2 \pi^2 t}{4L^2} \qquad \text{and} \qquad f = \frac{(2n+1)\pi}{2L} \quad .$$

Placing the independent parameters outside the integral, yields the following:

(21) $$K = 1 - \frac{4}{\pi B'} \int_0^L \sum_{n=0}^{\infty} \frac{(-1)^n}{2n+1} \exp(g) \cos(fz) \exp(-2\gamma z) dz$$

Recalling the law of summation of integrals, equation (21) may be rewritten as:

(22) $$K = 1 - \frac{4}{\pi B'} \sum_{n=0}^{\infty} \int_0^L \frac{(-1)^n}{(2n+1)} \exp(g) \cos(fz) \exp(-2\gamma z) dz$$

Placing the terms that are independent of z outside the integral and rewriting in terms of [E] gives,

(23) $$K = 1 - \frac{4}{\pi B'} * \sum_{n=0}^{\infty} \frac{(-1)^n}{(2n+1)} \exp(g)[E]$$

Integrating [E] by parts yields,

(24) $$[E] = \frac{\cos(fz)\exp(-2\gamma z)}{-2\gamma z}\Bigg|_0^L - \int_0^L \frac{\exp(-2\gamma z) f \sin(fz)}{2\gamma}$$

Once again, evaluating the integral by parts,

$$\frac{-f}{2\gamma} \int_0^L \exp(-2\gamma z) \sin(fz) dz = \frac{-f}{2\gamma} \left[\frac{\sin(fz)\exp(-2\gamma z)}{-2\gamma} \Bigg| - \int_0^L \frac{\exp(-2\gamma z)}{-2\gamma} f \cos(fz) dz \right]$$

(25)

Substituting equations (25) into (24),

$$[E] = \frac{\cos(fl)\exp(-2\gamma L) - 1}{-2\gamma} + \frac{f \sin(fl)\exp(-2\gamma L)}{(2\gamma)^2} + \frac{-f^2}{(2\gamma)^2} \int_0^L \cos(fz)\exp(-2\gamma z) dz$$

(26)

Recognizing that the remaining integral is identical to the original definition of [E], and simplifying yields,

$$(27) \qquad [E]\left(\frac{4\gamma^2 + f^2}{4\gamma^2}\right) = \frac{\cos(fl)\exp(-2\gamma L) - 1}{-2\gamma} + \frac{f\sin(fl)\exp(-2\gamma L)}{4\gamma^2}$$

Multiplying both sides by $\frac{4\gamma^2}{4\gamma^2 + f^2}$,

$$(28) \qquad [E] = \frac{\left[-2\gamma\cos(fl)\exp(-2\gamma L) + 2\gamma + f\sin(fl)\exp(-2\gamma L)\right]}{(4\gamma^2 + f^2)}$$

Recalling that $fl = \left(\frac{(2n+1)\pi}{2L}L\right)$,

$$(29) \qquad \cos(fl) = \cos\left(\frac{(2n+1)\pi}{2L}L\right) = \cos\left(\frac{(2n+1)\pi}{2}\right).$$

For n = odd, $\cos(fl) \Rightarrow 0$.
For n = even, $\cos(fl) \Rightarrow 0$.

Therefore, the cos(fl) term can be replaced by zero.
Considering the sine term,

$$(30) \qquad \sin(fl) = \sin\left(\frac{(2n+1)\pi}{2L}L\right) = \sin\left(\frac{(2n+1)\pi}{2}\right)$$

For n = odd, $\sin(fl) \Rightarrow -1$.
For n = even, $\sin(fl) \Rightarrow +1$.

Therefore, the sin(fl) term can be replaced by $(-1)^n$.
Upon making these substitutions,

$$(31) \qquad [E] = \frac{1}{\left(4\gamma^2 + f^2\right)}\left[2\gamma + (-1)^n f\exp(-2\gamma L)\right]$$

Recalling equations (14) and (23), K can be rewritten as:

(32) $$K = 1 - \frac{4}{\pi B'} \sum_{n=0}^{\infty} \frac{\exp(g)\left[2\gamma(-1)^n + (1) f \exp(-2\gamma L)\right]}{(2n+1)(4\gamma^2 + f^2)}$$

Therefore, the final expression is given as:

(33) $$\boxed{\frac{A_t}{A_\infty} = 1 - \frac{8\gamma}{\pi(1-\exp(-2\gamma L))} \sum_{n=0}^{\infty} \frac{\exp(g)\left[(-1)^n 2\gamma + f \exp(-2\gamma L)\right]}{(2n+1)(4\gamma^2 + f^2)}}$$

where A_t = absorbance at time *t*
A_∞ = absorbance at infinite time
γ = 1/dp = 1/ penetration depth
L = film thickness

$$g = \frac{-D(2n+1)^2 \pi^2 t}{4L^2} \qquad \text{and} \qquad f = \frac{(2n+1)\pi}{2L} \ .$$

This equation provides a means of quantitative analysis of FTIR-ATR data for the evaluation of diffusion kinetics. It also allows for adjustments of experimental parameters and emphasizes the *change* in absorbance with time. This derivation can be easily modified to accommodate other testing geometries, as long as the concentration profile is solved for the proper boundary conditions. The actual design, development, and use of an appropriate testing configuration, based upon the above model are discussed in the next section.

4.7 Design and Building of ATR Diffusion Cell

An ATR diffusion apparatus has been constructed based upon a horizontal IRE crystal flat-plate. The design for the experimental setup possesses the following criteria:

1) the ability to hold a liquid penetrant, yet has one open face to allow for direct exposure of the polymer film
2) dimensions appropriate to the ATR crystal flat-plate.
3) good temperature control with no “hot-spots”
4) large enough to minimize any “wall effects” that may occur from the sides of the diffusion chamber itself
5) convenient to clean and refill
6) easily secured to form a liquid-tight seal upon application of the clamping pressure.

The sample cell consists of a hollow rectangle whose inner dimensions are larger than those of the crystal. Therefore, the area of the film must be greater than the area of the crystal to prevent any penetrant from wicking through the sides into the polymer-crystal interface. According to Figure 4-9 and Figure 4-10, the dimensions of the reservoir resemble those of a bottomless box milled out of an aluminum block approximately 18 x 96 x 17 mm. Two 1/8" NPT valves have been inserted into the two ends for filling the cell with penetrant. The front side of the "box" contains two holes of 1.2 mm diameter for the passage of heater wires connected to a temperature controller (Omega CN900A in series with a 120V variable autotransformer). The heater is comprised of resistance wire coiled into a tiny spiral of approximately 5 mm in diameter that extends along the entire inside length of the reservoir. A K-type thermocouple whose calibration curve was meticulously established to insure accurate readings, was placed at the exit NPT valve for monitoring the temperature. A schematic of the horizontal-ATR penetrant cell used is given in Figure 4-11.

A second means of temperature control is provided by the penetrant loading mechanism itself. The NPT valves are connected to 1/8" copper tubing with a T-joint on the exit side to allow insertion of the thermocouple wire. The copper tubing is highly insulated and leads to an external polypropylene container. The penetrant is placed in this container and allowed to equilibrate to the test temperature inside a Hewlett-Packard 5890 GC oven. This setup is in series with a liquid pump that cycles the penetrant into the reservoir at a rate of 10 cc/min. A constant flow rate is used for all experiments, and the T-joint at the exit of the reservoir minimizes the pressure that may develop. The entire testing apparatus is shown in Figure 4-12.

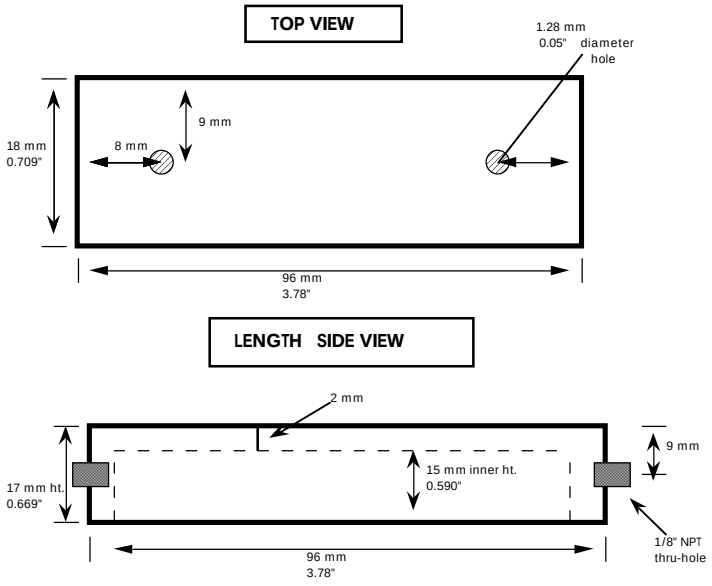

Figure 4-9. Schematic of the Liquid ATR Diffusion Cell

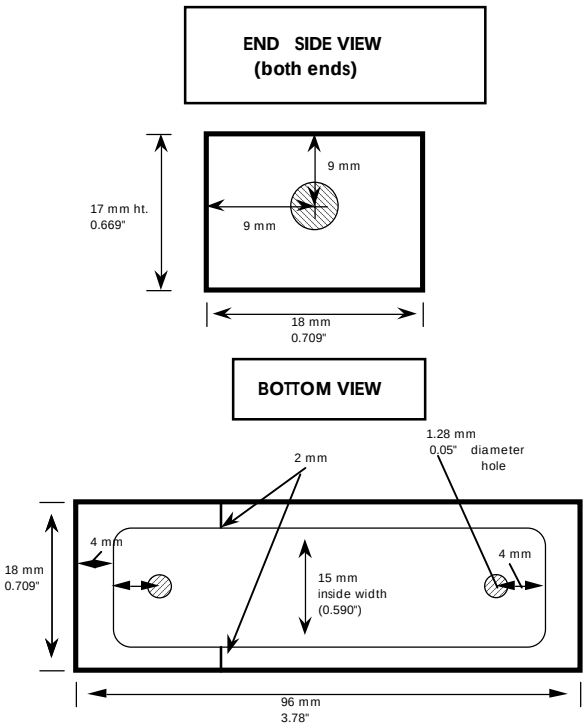

Figure 4-10. Continued Schematic of Liquid ATR Diffusion Cell

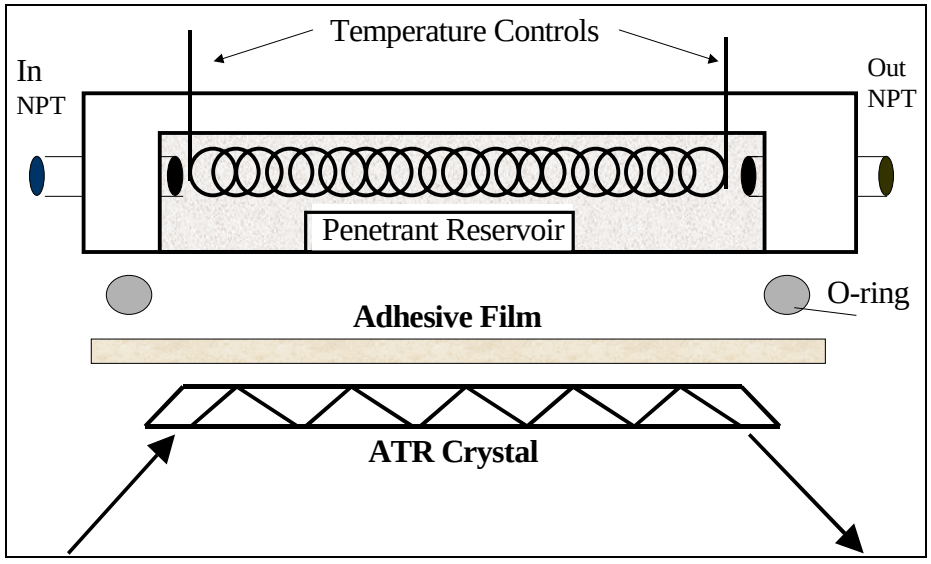

Figure 4-11. Cross-section of the Liquid ATR-Diffusion Cell with Adhesive Film Shown

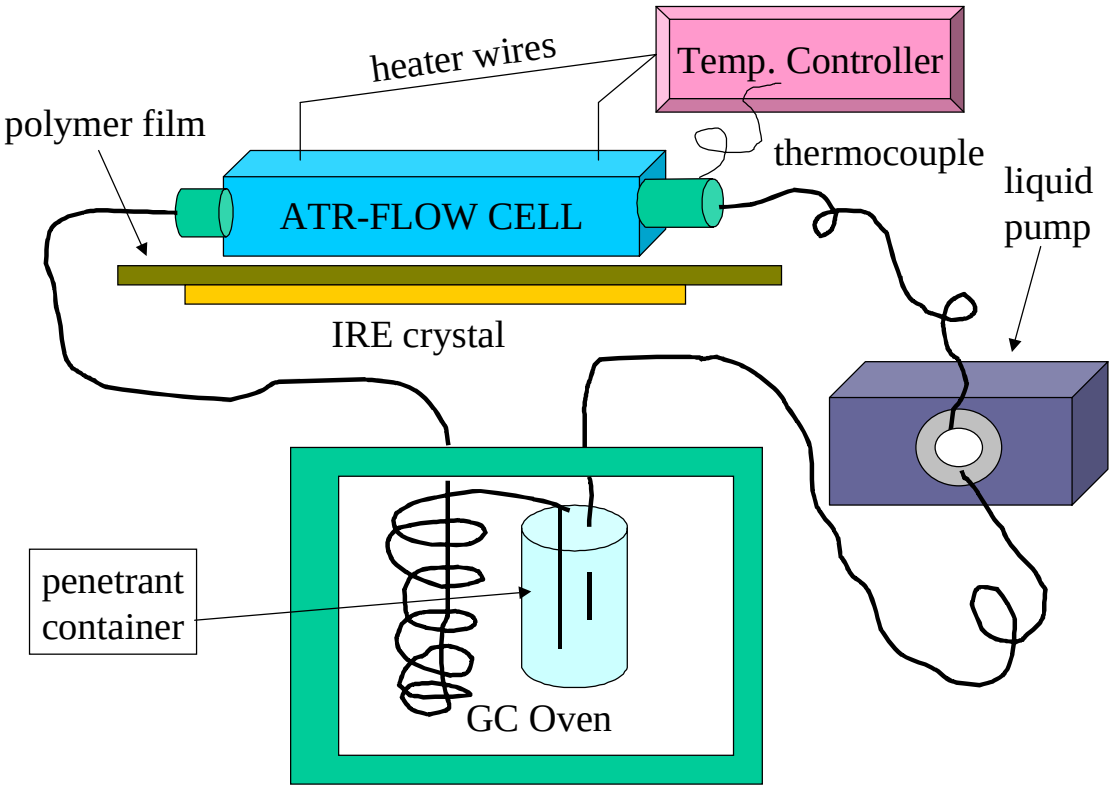

Figure 4-12. External schematic of entire ATR setup

4.8 Optical Property Evaluation

The development of a Fickian-based FTIR-ATR model and its application to the designing of the ATR apparatus has been discussed in the previous section. Prior to any quantitative experimentation, accurate values for optical constants and depth of penetration, d_p, must be evaluated. Recalling the expression for d_p, the dependence upon the wavelength of interest and the refractive indices of both the IRE crystal (n_1), and polymer (n_2). Since optical properties for polymers in the infrared region of the spectrum are scarce in the literature, n_2 of the polymer needs to be evaluated experimentally.

One of the methods for determining refractive indices of unknown polymers is that proposed by Harrick[70] and involves identifying the critical angle, θ_c, for a material. This angle is defined as the minimum angle of incidence required to produce total internal reflection of an optical wave, and is expressed by equation (34).

(34) $$\theta_c = \sin^{-1}\left(\frac{n_2}{n_1}\right)$$

where n_1 = refractive index of the waveguide
and n_2 = refractive index of the sample medium.

Absorbance spectra are collected at variable angles using an IRE in intimate contact with the polymer. A distorted refractive index dispersion occurs, instead of a *normal* spectrum (similar to transmission) at θ_c.

In order to measure θ_c, a film of the polymeric adhesive was mounted and clamped onto a variable angle reflection accessory (5° to 85°; ±0.5°) known as a *Seagull*™ (Harrick Scientific Corporation) *reflection attachment*. This attachment is a multipurpose unit that was used in a single reflection mode through a Zinc Selenide (ZnSe) hemispherical crystal in conjunction with a *Nicolet 510 spectrophotometer* (4cm^{-1} resolution). Spectra were collected as a function of incident angle in increments 2°, and were averages of 120 scans collected with a triglycine sulfate (TGS) detector. Experimental data for the R/flex 410 adhesive are shown below for various angles (Figure 4-13). Characteristic peaks in the 1600-1800 cm^{-1} region were monitored for optical dispersion, the range of interest for the kinetic experiments.

A critical angle of 41 ± 1° was determined for the polymer from the onset of refractive index dispersion. Using equation (34) and n_1= 2.40 for ZnSe, the index of refraction for the R/flex material, n_2, was calculated to be 1.5745 ± 0.0316. This value is representative of the wavelength range studied, since refractive index is known to depend strongly upon wavelength. In addition, d_p was estimated to be equal to 1.449 ±0.2 μm, based on an angle of incidence of 45°. It was observed that d_p showed a negligible dependence on θ_c. This result is in accordance with those of Skourlis and McCullough[71] and justifies the optical constant evaluation method used.

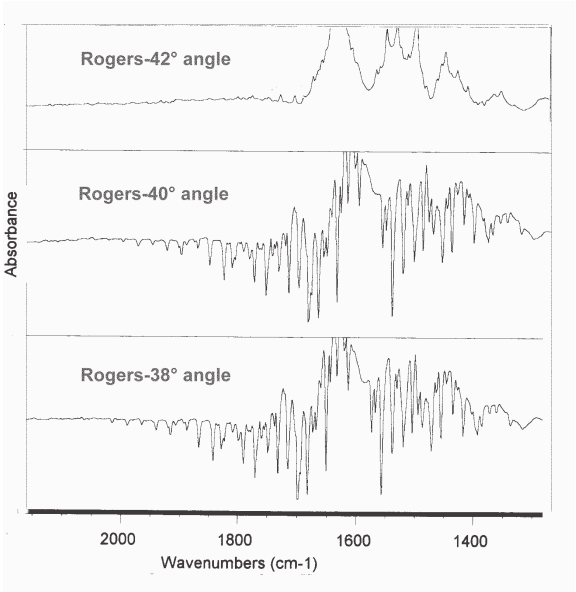

Figure 4-13. R/flex 410 Spectrum Variation with Angle of Incidence. Transition from normal absorption to refractive index dispersion.

4.9 Data Analysis

4.9.1 Simplex Methodology

The data analysis was based on a linear programming technique developed by G.B. Dantzig[72,73,74] in the late 1940's, known as the *simplex* method. This method involves two phases:

> Phase I- find an initial, *basic feasible solution* with only *m* nonzero variables X_i, that are positive (or zero),
> Phase II- try several solutions until an optimum is found.

This is done by evaluating the *residual error*, and then scaling each guess by a predetermined factor, creating a centroid in an x-y plane. The errors from all the coordinates along the newly created centroid are compared, and the one with the least error is used as the next "initial guess". The process is repeated as the algorithm quickly converges on a path towards the nearest minimum. Therefore, selection of the scaling factor is crucial in determining the true global minimum of an equation. The Fortran code written for this purpose is listed in Appendix D.

4.10 Testing of Linear Programming

The ATR-diffusion model derived in section 4.6 is described by the following infinite sum over the number of terms, *n*.

$$\frac{A_t}{A_\infty} = 1 - \frac{8\gamma}{\pi(1-\exp(-2\gamma L))}\sum_{n=0}^{\infty}\frac{\exp(g)\left[(-1)^n 2\gamma + f\exp(-2\gamma L)\right]}{(2n+1)(4\gamma^2 + f^2)} \quad (33)$$

In order to shorten computation time, it was beneficial to determine the *n* that would yield the most accurate diffusion coefficients. Therefore, an analysis of the sensitivity of the model to the *n* utilized was done, based on approximate values of wavelength, depth of penetration, and diffusion coefficients, D. The values of D ranged from 10^{-8}-10^{-10} cm^2/sec and were obtained from the mass uptake experiments that will be discussed in the next chapter. It can be seen from a plot of A_t/A_∞ vs. time, for various *n* terms (Figure 4-14), that the solutions begin to converge for $n > 100$. In our analyses, the number of summations, n, was chosen as 10,000, and was sufficient to yield accurate results.

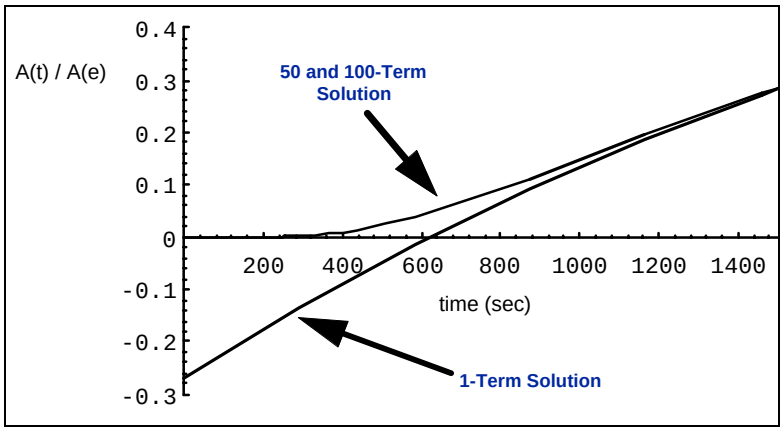

Figure 4-14. Minimization in the number of terms *n* for the ATR - Diffusion Model of equation (33).

The optimization technique was tested using literature data from the diffusion of water in polyacrylonitrile (PAN)[75] at 102°C and 57°C. Values for D and A_∞, spanning a large range, were allowed to converge towards an optimum value, in order to determine the true global minimum. The initial guesses for both D and A_∞ versus residual error (S) are plotted three-dimensionally, showing this minimum (Figure 4-15). Such an analysis was employed in the evaluation of diffusivities, throughout this research.

A comparison of the 102°C water-PAN literature data and those generated from the above procedure are shown in Figure 4-16. It can be seen that there is excellent agreement between the two. Furthermore, literature values of D and A_∞ of 1.236 x 10^{-10} cm^2/sec and 337.55, respectively, were consistent with the simulated results of 1.232 x 10^{-10} cm^2/sec and 330.98. This provides ample evidence that analytical methods developed are highly accurate for the analysis of the R/flex 410 polymer adhesive studied in this present investigation.

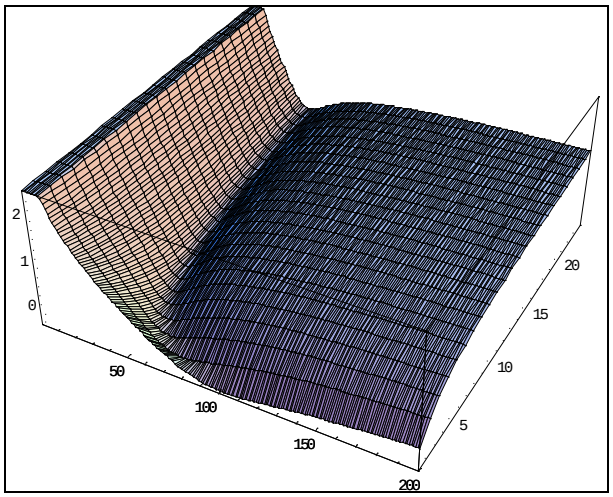

Figure 4-15. Plot of log residual (*S*) vs. Diffusivity and A_∞ (x,y, and z respectively). Note that on the x and y axes are provided arbitrary units for illustration.

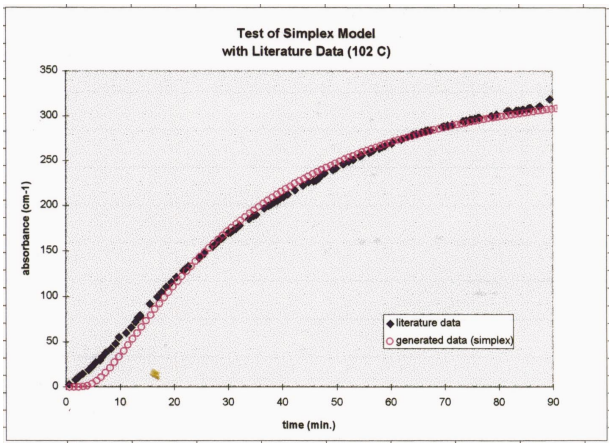

Figure 4-16. Simplex Fit of PAN 102°C Literature Data (ref. 32)

4.11 Results and Discussion

The results obtained from the FTIR-ATR studies on the polymer-penetrant systems will be discussed below.

4.11.1 Analysis of Absorption Spectra

An ATR spectrum for the neat R/flex polymer adhesive is shown (Figure 4-17). The characteristic amide peaks seen in this spectrum are:

1) the amide I band at ~1640 cm^{-1} (6.10μ), resulting from the C=0 stretching of the polyamide linkage.
2) the amide II band at ~1545 cm^{-1} (6.50 μ), indicative of a bending deformation between the N-H bond.
3) the amide III band at ~1300 cm^{-1} (7.79μ), characteristic only of secondary amides.
4) a strong absorption due to the N-H stretching of the amide linkage that is shifted to a lower frequency of about 3300 cm^{-1} (3.03μ), and
5) its twin N-H stretch at 2950 cm^{-1} (3.39μ).

Other key spectral features are those of the broad C-H epoxide vibration near 940 cm^{-1} and 1250 cm^{-1}.

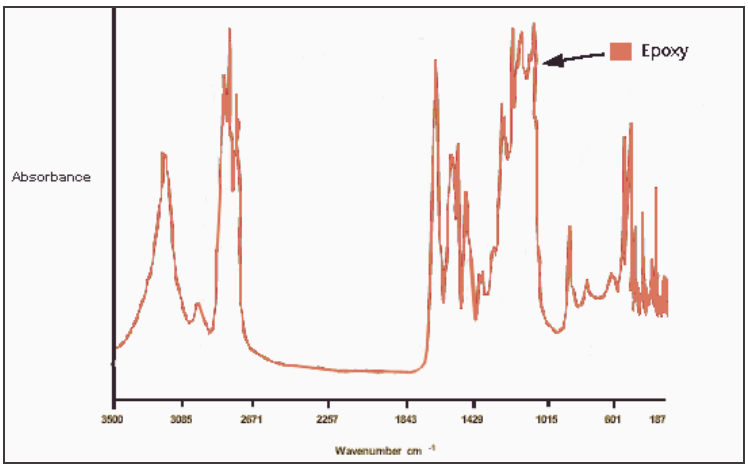

Figure 4-17. IR Spectrum of R/flex 410 Adhesive Material

Figure 4-18 shows a comparison of the spectra of the polymer and one of the ester penetrants studied-isodecyl pelargonate (IDP). It can be seen that that the carbonyl stretching of the ester at 1735cm^{-1} is very prominent and free of interference from any other bands. As a result, this peak will be monitored to follow the kinetics of the diffusion processes, *in-situ*.

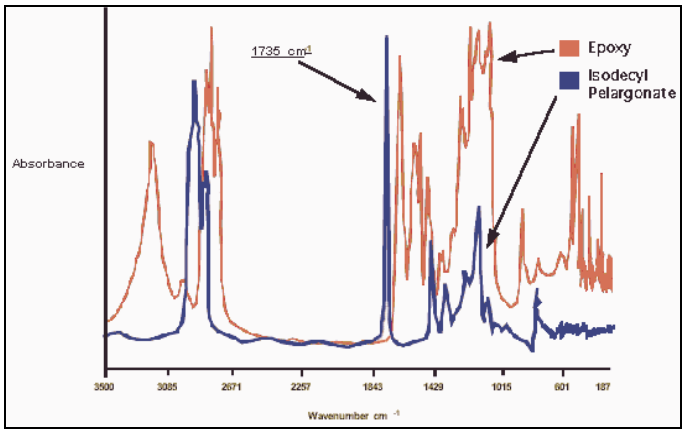

Figure 4-18. Overlay of Isodecyl Pelargonate and R/flex 410 Adhesive Material

Due to the sensitive nature of the technique, variations in film thickness could be a primary source of error. As a result, these effects were studied in detail. Simulations of a normalized absorbance spectrum as a function of thickness (L) are shown in Figure 4-19. It can be seen that the absorbance curve depends greatly upon L. In an effort to minimize error, all films used were 1.5 mils thick, except for IDP, whose film thicknesses were 0.5 mils, to aid in shortening the lengthy experimental times.

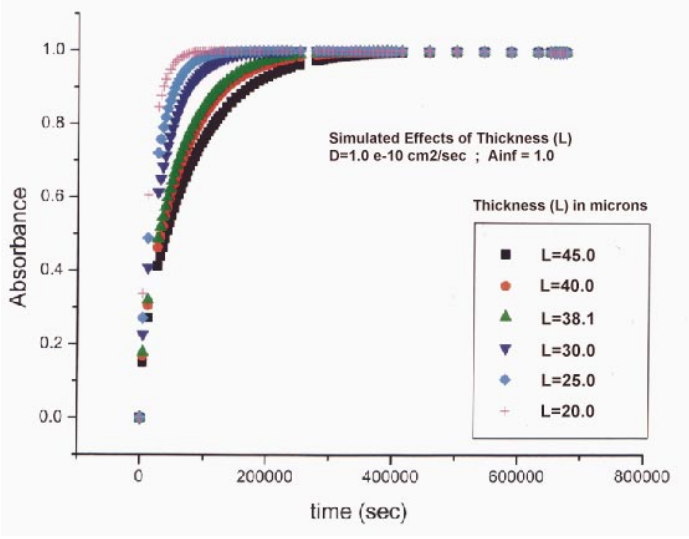

Figure 4-19. Simulation of Thickness Dependence

Before the polymer film was exposed to the penetrants, it was isothermally equilibrated for 20 minutes, and its IR spectrum was collected and used as the reference (t=0). As the liquid filled the film chamber, the spectra were automatically obtained at designated time intervals. The experimental spectra for IDP at room temperature at various times are shown in Figure 4-20. The growth of the 1735 cm^{-1} peak as a function of time can be seen.

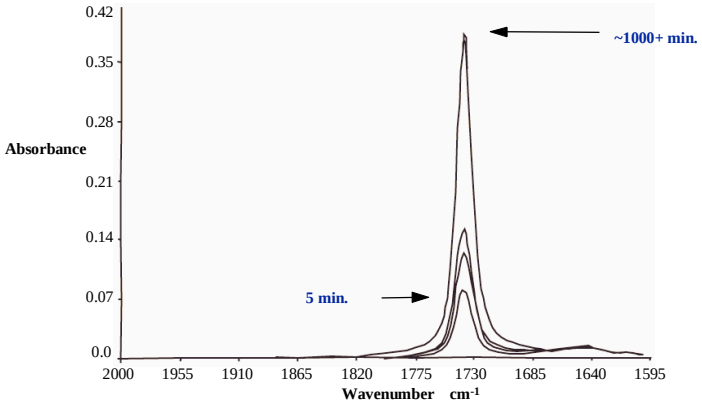

Figure 4-20. In-situ Monitoring of Ester Diffusion (IDP at 23°C)

Quantitative analysis was achieved by ratioing the peak height of the 1735 cm^{-1} ester band to the 1640 cm^{-1} polymer peak that remained constant throughout the study. Such a ratio compensates for any variations in the degree of contact between the film and crystal that may have occurred. Diffusion coefficients, D, and A_∞, were evaluated from the normalized data using the simplex algorithm and found to be 4.94 x 10^{-11} cm^2/sec and 0.262, respectively, for IDP. The experimental data is compared to the simulated results in Figure 4-21. All residual errors (S) were minimized to insure an optimum fit as shown in Figure 4-22.

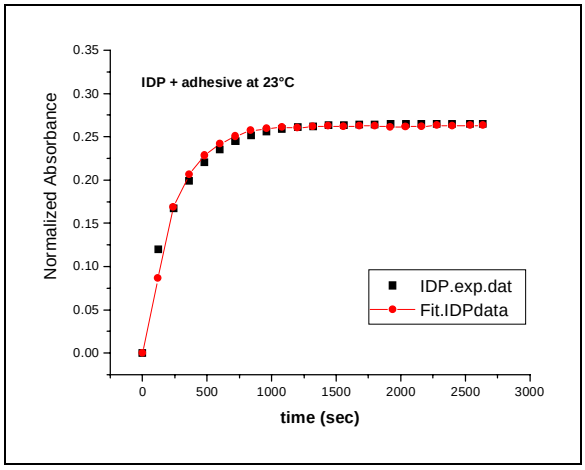

Figure 4-21. Optimized Fit of IDP + Polymer Experimental Data (23°C)

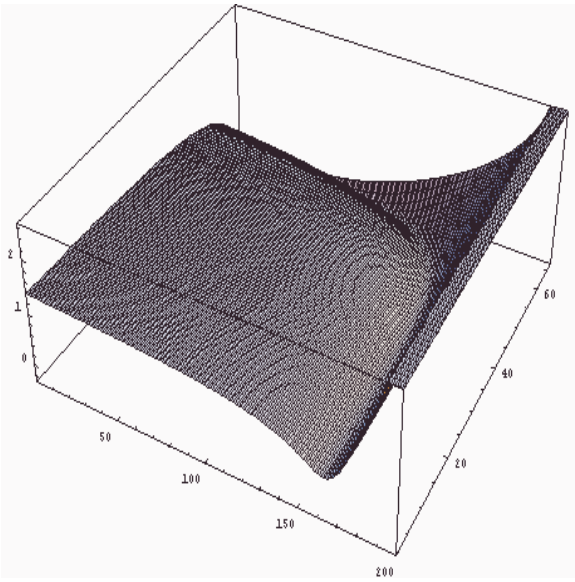

Figure 4-22. Plot of log S (residual error) vs. Diffusivity and A_∞ Diffusion (x,y, and z respectively) for IDP. Note that on the x and y axes are provided arbitrary units for illustration.

This analysis was repeated for all the penetrants at room temperature. The results are shown in Figure 4-23 through Figure 4-26 and in Table 4-2. Since no literature data is available for these systems, the diffusion coefficients evaluated above will be compared to those from the kinetic mass uptake experiments at different temperatures in the next chapter.

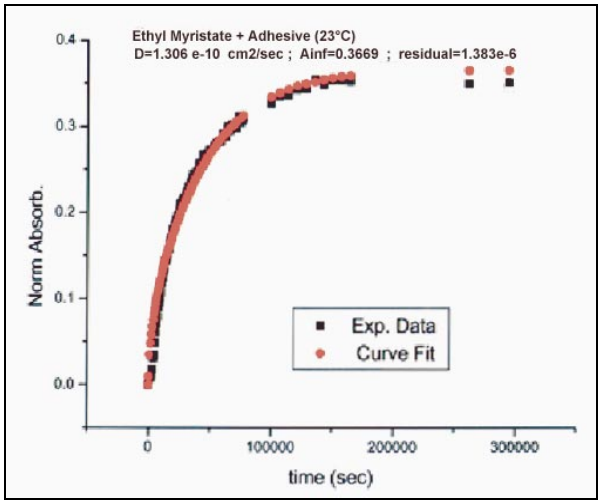

Figure 4-23. IR Diffusion Data and Curve Fit for Ethyl Myristate (23°C)

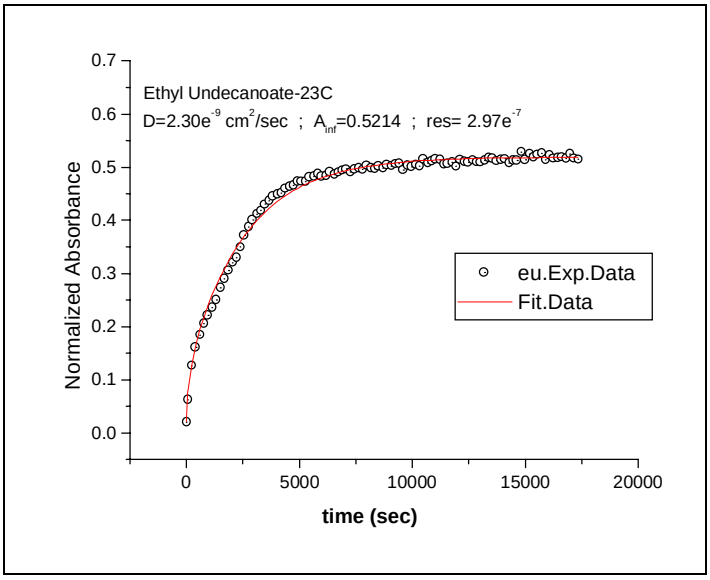

Figure 4-24. IR Diffusion Data and Curve Fit for Ethyl Undecanoate (23°C)

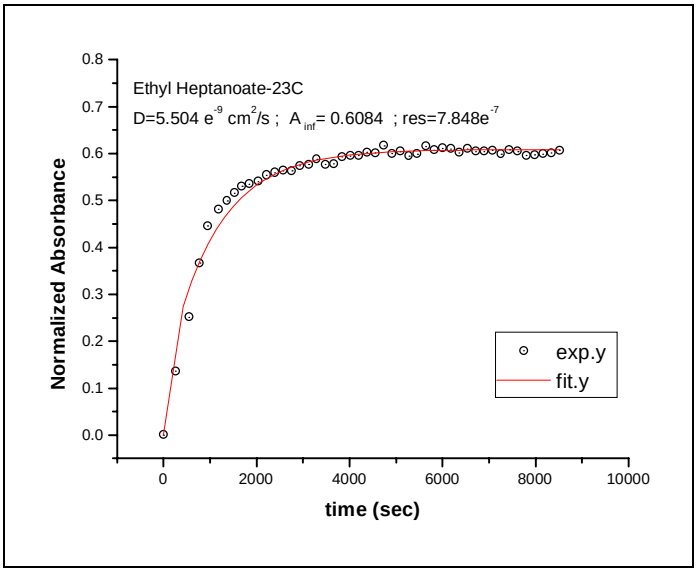

Figure 4-25. IR Diffusion Data and Curve Fit for Ethyl Heptanoate (23°C)

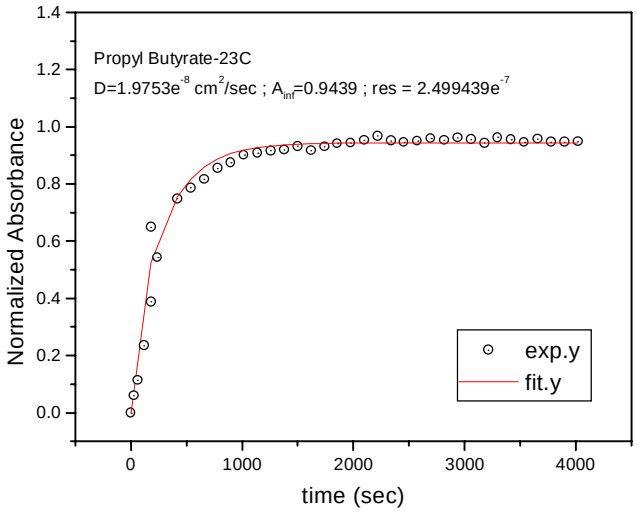

Figure 4-26. IR Diffusion Data and Curve Fit for Propyl Butyrate (23°C)

Table 4-2. Evaluated Diffusivity (cm^2/sec) and Equilibrium IR Absorption of Ester Penetrants in R/flex 410 via FTIR-ATR Spectroscopy

Sample	IDP (D)	A_∞	EM (D)	A_∞	EU (D)	A_∞
1	$4.94e^{-11}$	0.2622	$1.31e^{-10}$	0.3669	$1.81e^{-9}$	0.5214
2	$1.03e^{-10}$	0.3214	$1.92e^{-10}$	0.4130	$2.30e^{-9}$	0.5420
3	$8.31e^{-11}$	0.2742	x	x	x	x
Ave:	$7.85e^{-11}$	0.2859	$1.62e^{-10}$	0.3900	$2.06e^{-9}$	0.5317
std.dev.	$2.71e^{-11}$	0.0313	$4.31e^{-11}$	0.0326	$3.46e^{-10}$	0.0146

Sample	EN (D)	A_∞	EH (D)	A_∞	PB (D)	A_∞	EP (D)	A_∞
1	$4.23e^{-9}$	0.6210	$8.02e^{-9}$	0.6147	$1.98e^{-8}$	0.9439	$1.81e^{-8}$	1.050
2	$5.02e^{-9}$	0.6140	$5.50e^{-9}$	0.6084	x	x	x	x
Ave:	$4.63e^{-9}$	0.6175	$6.76e^{-9}$	0.6116	$1.98e^{-8}$	0.9439	$1.81e^{-8}$	1.050
std.dev.	$5.59e^{-10}$	0.0049	$1.78e^{-9}$	0.0045				

x-data not obtained due to lack of material

A plot of diffusivity, D, versus molar mass for the esters is shown in Figure 4-27. A general increase in D with decreasing molecular weight of the ester is observed, consistent with other literature[76,77,78,79]. This is due to the ease of accommodation of the lower molecular weight species by the polymer matrix, requiring less complex motions of chain segments during the transport process.

One of the key features of this *in-situ* FTIR-ATR technique is its unique ability to provide chemical as well as kinetic information. Attempts were made to study any specific interactions that may have occurred during the transport process. In particular, the amide I and II peaks have been analyzed for any indications of possible dipole or acid-base interactions between the polar ester and polar polymer matrix.

The equilibrium values for normalized absorbance, A_∞, show a strong dependence upon the polarity of the penetrant molecules. This can be seen in a plot of A_∞ versus the solubility parameter of each species shown in Figure 4-28. The maximum A_∞ corresponded to the most polar, lowest molecular weight ester penetrant, ethyl propionate.

A plot of the chemical shifts $\Delta\nu$ (cm^{-1}) as a function of time for these amide bands are shown in Figure 4-29 and Figure 4-30. General trendlines have been drawn through each set of data to allow for visual comparison. Qualitatively, $\Delta\nu$ increases toward lower wavenumbers of absorption as the polarity of the low molecular weight species increases. This implies that ethyl propionate (EP) is the most soluble ester, and is consistent with the highest A_∞ corresponding to EP, as described above. However, the longer, flexible alkyl substituents may be able to more easily obtain conformations that result in "shielding" of the ester carbonyl from the polar polyamide moieties[80]. This could also result in a "dilution" of the polarity of the ester, as reflected in the decreasing solubility parameters[81].

Arrhenius kinetics were used to analyze the temperature dependence of the transport of IDP into the polymer (Table 4-3). The activation energy, E_d, was evaluated to be ~83.9 kJ/mole, much greater than that for a typical pore-type diffusion. This could be due to an enhanced mobility of polymer chains as a result of the low T_g allowing *more* polymer segments to become involved in the process. This value of E_d will also be compared to the E_d evaluated from kinetic mass uptake experiments described in Chapter 5.

Table 4-3. Temperature Dependence of IDP Diffusivity via FTIR-ATR Spectroscopy

Temperature (°C)	Log D (cm2/sec)
27	-9.12
33	-8.60
40	-8.30
50	-8.05

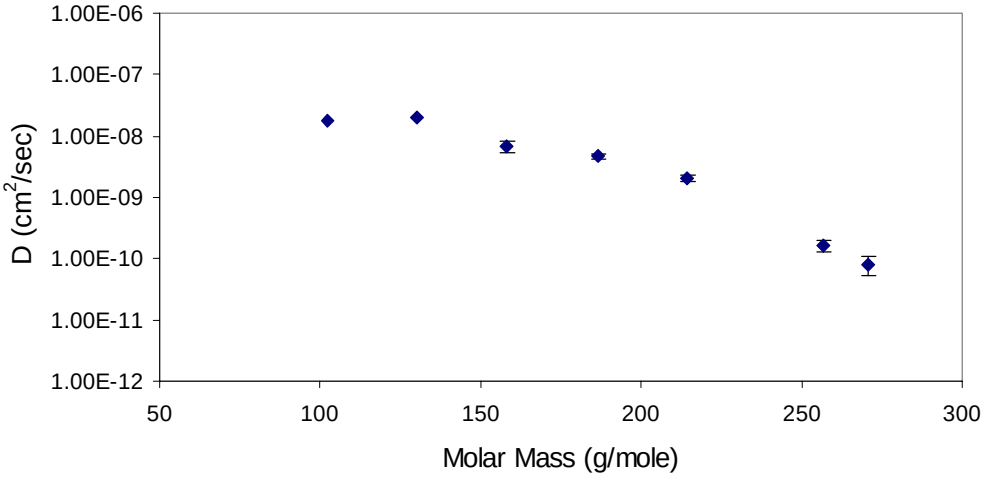

Figure 4-27. Diffusivity vs. Molecular Size of Ester Penetrants (23°C)

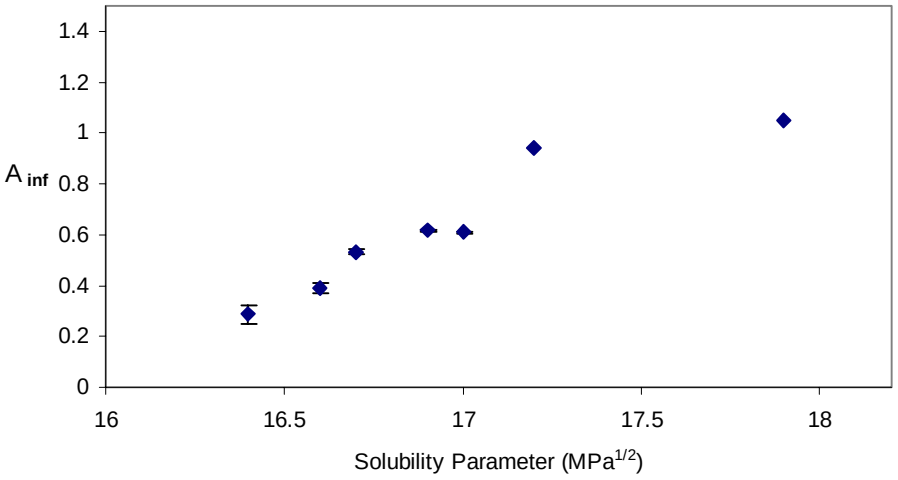

Figure 4-28. Equilibrium IR Absorbance vs. Solubility Parameters of Esters

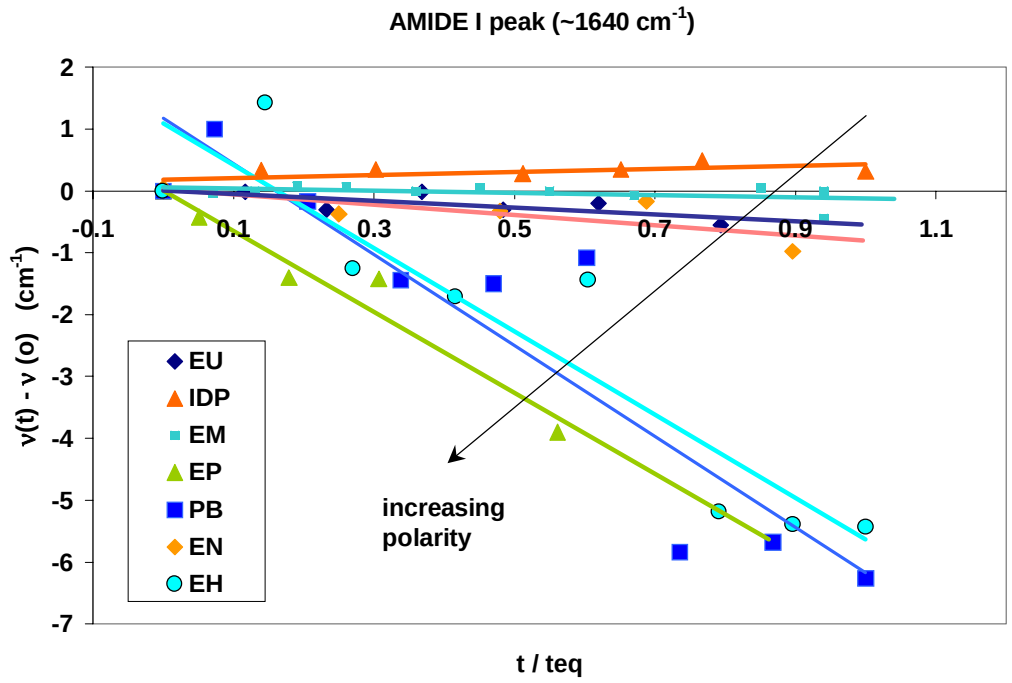

Figure 4-29. Chemical Shifts of Amide I Absorption (~1640 cm^{-1}) as a Function of Exposure Time to Ester Penetrants.

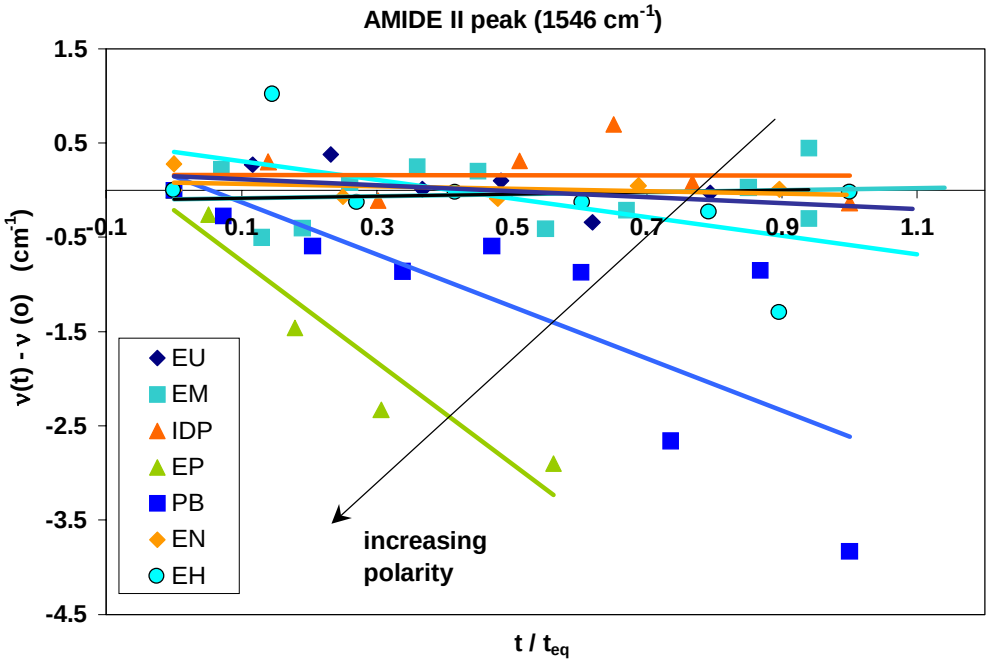

Figure 4-30. Chemical Shifts of Amide II Absorption (~1547 cm^{-1}) as a Function of Exposure Time to Ester Penetrants

4.12 Summary

An FTIR-ATR based method for monitoring diffusion processes, in-situ, has been successfully implemented. Mathematical models relating diffusion to the physics of infrared spectroscopy have been devised. Computer programs have been written for numerical optimization of experimental data to evaluate the diffusion coefficients and equilibrium absorbance, A_∞, values. The esters studied exhibited a dependence of diffusivity on molecular size. The *in-situ* procedure and analysis have provided excellent results at much shorter experimental times than other conventional techniques.

In addition to the transport coefficients, this method has also provided a wealth of chemical information. Characteristic peaks allowed monitoring of individual functionalities during the kinetic process. Due to its quantitative nature, the A_∞ values are proportional to the equilibrium solubilities of the penetrants within the polymer. Correlations relating A_∞ and solubility parameters have been made. These indicate that weak, specific interactions exist between the amide linkage (in polymer) and ester moiety, and become stronger with increasing polarity of the penetrant. The analysis of chemical shifts induced by the polar esters also leads to the same conclusion.

Unfortunately, additional experiments could not be performed due to inconsistencies and defects in the polymer films available for this investigation. Since this particular testing configuration has proven to be extremely sensitive to film quality, any defects in the film will result in inaccurate diffusion coefficients. However, this sensitivity may be used to its advantage as a quality-control technique for monitoring film quality.

The above results may be utilized in conjunction with mass uptake experiments, to investigate the structural and chemical effects on the transport process, as will be described in the next chapter.

Endnotes

[1] F.M. Mirabella, "Principles, Theory, and Practice of Internal Reflection Spectroscopy," Internal Reflection Spectroscopy-Theory and Applications, ed. F.M. Mirabella, Jr., Marcel Dekker, Inc. New York. (1993).
[2] T.P.Skourlis and R.L. McCullough, *Journal of Applied Polymer Science*, 52, 1241-1248 (1994).
[3] R.H. Renard, *Journal of Optical Society of America*, 54, 1190 (1964).
[4] T. Hirschfield, *Applied Spectroscopy*. 31, 243 (1977).

[5] D.J. Epstein, *Applied Spectroscopy* 34 233 (1980).
[6] N.J. Harrick and F.K. duPre, *Applied Optics* 5, 1739 (1966).
[7] F.M. Mirabella, *Journal of Polymer Science, Polymer Physics Edition*,. 21 2403 (1983).
[8] D.J. Carlsson and D.M. Wiles, *Canadian Journal of Chemisty*, 48, 2397 (1970).
[9] R. Iwamoto and K. Ohta, *Applied Spectroscopy*, 38, 359 (1984).
[10] E.Hecht and A. Zajac, Optics, Chapt.3, Addison-Wesley, Reading 1974.
[11] F.M. Mirabella, Jr., *Journal of Polymer Science, Polymer Physics Edition*, 22, 1283 (1984).
[12] R.T.Graf, J.L.Koenig, and H.Ishida, 39, 3, 405-408 (1985).
[13] R.G. Greenler, *Journal of Chemical Physics*, 44, 310 (1966).
[14] S.A. Francis and A.H. Ellison, *Journal of the Optical Society of America*, 49, 131 (1959).
[15] Koichi Nishikida and R.W. Hannah, *Applied Spectroscopy* 46, 6 (1992).
[16] D.L. Allara, A.Baca, and C.A. Pryde, *Macromolecules*, 11, 1215 (1978).
[17] R.T.Graf, J.L. Koenig, and J.Ishida, Fourier Transmission Infrared Characterization of Polymers, ed. H. Ishida, Plenum Press, New York, 1987.
[18] N.J.Harrick, Internal Reflection Spectroscopy, Interscience Publishers, New York, 1973.
[19] L.J. Janik, *Applied Spectroscopy*, 40, 661, (1986).
[20] J.B.Huang and M.W. Urban, *Applied Spectroscopy* 46, 6, 1014-1019 (1992).
[21] T.B. Hirshfield, *Analytical Chemistry*, 48, 721 (1976).
[22] J.L. Koenig, *Advanced Polymer Science*, 54, 87 (1983).
[23] K.C.Farinas, L.Doh, S.Venkatraman, and R.O.Potts, *Macromolecules*, 27, 5220-5222 (1994).
[24] F.M. Mirabella, *Journal of Polymer Science, Polymer Physics Edition*, 22, 1293- 1301 (1984).
[25] P. Yuan and C.S.P. Sung, *Macromolecules*, 24, 6095- 6101 (1991).
[26] E.J. Vorenkamp, J. van Ruiten, F.A. Kroesen, J.G. Meyer, J. Hoekstra, and G. Challa, *Polymer Communications*, 30, 116 (1989).
[27] N.A. Remizov, A.Y. Chalykh, V.Y. Popov, and V.V. Lavrent'ev, *Vysokomol. Soedin*, A24, 1853 (1982).
[28] H.H. Kausch and K. Jud, *Proceedings of 28th IUPAC Macromolecule Symposium*, 717 (1982).
[29] J.Crank, The Mathematics of Diffusion, Oxford Univerisity Press, Oxford, 1956.
[30] N.E. Schlotter and P.Y. Furlan, *Vibrational Spectroscopy* 3, 147-153 (1992).
[31] P.Y. Furlan, *Macromolecules* 25, 6516-6522 (1992).
[32] G.T. Fieldson and T.A. Barbari, *Polymer*, 34, 6, 1146-1153 (1993).
[33] E.Sacher and J.R. Susko, *Journal of Applied Polymer Science*, 23, 2355 (1979).
[34] E. Sacher and J.R. Susko, *Journal of Applied Polymer Science*, 26, 679 (1981).
[35] D.K. Yang, W.J. Koros, H.B. Hopfenberg, and V.T. Stannet, *Journal of Applied Polymer Science*, 30, 1035 (1985).
[36] D.K. Yang, W.J. Koros, H.B. Hopfenberg, and V.T. Stannet, *Journal of Applied Polymer Science*, 31, 1619 (1986).
[37] C.R. Moylan, M.E. Best, M.J. Ree, *Journal of Polymer Science, Part B: Polymer Physics*, 29, 87 (1991).
[38] K, Okamoto, N.Tanihara, and H.Watanabe, K. Tanaka, K. Hidetoshi, A. Nakamura, Y. Kusuki, and K. Nakagawa, *Journal of Polymer Science, Part B: Polymer Physics*, 30, 1223 (1992).
[39] G. Xu, C.C. Gryte, A.S. Nowick, S.Z. Li, Y.S. Pak, S.G. Greenbaum, *Journal of Applied Physics*, 66, 5290 (1989).
[40] B.S. Lim, A.S. Nowick, K.Lee, A.J. Viehbeck, *Journal of Polymer Science, Part B: Polymer Physics*, 31, 545 (1993).

[41] K.C. Farinas, L.Doh, S. Venkatraman, and R.O. Potts, *Macromolecules*, 27, 5220-5222 (1994).
[42] V.Y. Popov, V.V. Lavrent, *Journal of Applied Spectoscopy*, 32, 193 (1980).
[43] T. Nguyen, E. Byrd, and C. Lin, *Journal of Adhesion and Science Technology*, 5, 9, 697-709 (1991).
[44] T. Nguyen, D. Bentz, and E.Byrd, *Journal of Coatings Technology*, 66, 834, 39-50 (1994).
[45] T. Nguyen, D. Bentz, and E. Byrd, 67, 844, 37-46 (1995).
[46] G. Muller, K. Abraham, and M. Schaldach, *Applied Optics*, 20, 1182-1190 (1981).
[47] T.P. Skourlis and R.L. McCullough, *Journal of Applied Polymer Science*, 52, 1241-1248 (1994).
[48] S.U. Hong, T.A. Barbari, and J.M. Sloan, *Journal of Polymer Science, Part B: Polymer Physics*, 36, 337-344 (1998).
[49] S.H. McKnight and J.W. Gillespie, Jr., *Journal of Applied Polymer Science*, 64, 1971-1985 (1997).
[50] G.T. Fieldson and T.A. Barbari *AIChE Journal*, 41, 4, 795-804 (1995).
[51] R.A., Grinsted, L. Clark, and J.L. Koenig, *Macromolecules*, 25, 1235- (1992).
[52] E.D. von Meerwall, *Journal of Chemical Physics*, 54, 1-12, (1984).
[53] S.F. Tead, E.J. Kramer, *Macromolecules*, 21, 1513, (1988).
[54] F.J. Beuche, *Journal of Chemical Physics*, 48, 1410-1419 (1968).
[55] F.J. Beuche, *Journal of Chemical Physics*, 25, 599-604, (1956).
[56] S. Whitlow and R.P. Wool, *Macromolecules*, 24, 5926-5938 (1991).
[57] M.S. High, P.C. Painter, and M.M. Coleman, *Macromolecules*, 25, 797-801 (1992).
[58] E.A. Jordon, R.C. Ball, A.M. Donald, L.J. Fetters, R.A. Jones, and J. Klein, *Macromolecules*, 21, 235-239 (1988).
[59] S.H. McKnight, T.P. Skourlis, R.L. McCullough, and J.W. Gillespie, Jr., *Proceedings from the 9th Annual American Society of Composites*, Newark, DE., Sept., 1994.
[60] J.G. van Alsten and S. Lustig, *Macromolecules*, 25, 5069-5073 (1992).
[61] E. Jabbari and N.A. Peppas, *Macromolecules*, 26, 2175-2186 (1993).
[62] S.R. Lustig, J.G. van Alsten, and B. Hsiao, *Macromolecules*, 26, 3885-3894 (1993).
[63] J.G. van Alsten, S.T. Lustig, and B. Hsiao, *Macromolecules*, 28, 3672-3680 (1995).
[64] M.Muthukumar and A. Baumgartner, *Macromolecules*, 22, 1937 (1989).
[65] D.J. Crofton and R.A. Pethrick, *Polymer*, 22, 1048-1053 (1981).
[66] E.D. Meerwall, S.Amelar, M.A. Smeltzly, and T.P. Lodge, *Macromolecules*, 22, 295-304 (1989).
[67] B.W. Ludwig and M.W. Urban, *Polymer*, 1992.
[68] Y. Gao and P.R. Ogilby, *Macromolecules*, 25, 4962-4966 (1992).
[69] Crank, J. *Mathematics of Diffusion*, Clarenden Press, Oxford, 1979.
[70] N.J. Harrick, Internal Reflection Spectroscopy, Harrick, Ossining, New York, 1979.
[71] T.P. Skourlis and R.L. McCullough, *Journal of Applied Polymer Science*, 52, 1241-1248 (1994).
[72] G.B. Dantzig. Programming in a Linear Structrure, Comptroller, USAF, Washington, D.C., 1948.
[73] G.B. Dantzig. Linear Programming and Extensions. Princeton University Press, Princeton, N.J. 1963.
[74] Garret. N. Vanderplaats. Numerical Optimization Techniques for Engineering Design- with applications. McGraw-Hill Book Co. New York. 1984.
[75] G.T. Fieldson and T.A. Barbari. *Polymer* 34, 6, 1146- 1151 (1993).
[76] T.J. Aminabhavi and R.S. Khinnavar, *Polymer*, 34, 5, 1006-1018 (1993).
[77] K.Möller and T. Gevert, *Journal of Applied Polymer Science*, 51, 895-903 (1994).
[78] P.Meares, Polymers: Structures and Bulk Properties, van Nostrand, London. (1965).
[79] Handbook of Polymer Science, ed. J. Brandrup and E.H. Immergut, Wiley-Interscience, New York. 1989.
[80] J. Koszinowski, *Journal of Applied Polymer Science*, 31, 2711-2720 (1986).
[81] CRC Handbook of Solubility Parameters and Other Cohesion Parameters, 2nd ed., ed. A.F.M. Barton, CRC Press, Boca Raton. 1991.